Leave no stone unturned: The hidden potential of carbon and nitrogen cycling by novel, highly adapted *Thaumarchaeota* in the Atacama Desert hyperarid core

Running Title: *Thaumarchaea* in the hyperarid core of the Atacama

Yunha Hwang[1], Dirk Schulze-Makuch[1*], Felix L. Arens[1], Johan S. Saenz[3], Panagiotis S. Adam[2], Till L. V. Bornemann[2], Alessandro Airo[1], Michael Schloter[3], Alexander J. Probst[2*]

*corresponding authors

Affiliations:

[1] Center of Astronomy & Astrophysics, Technical University Berlin, 10623, Berlin, Germany.

[2] Environmental Microbiology and Biotechnology, Department of Chemistry, University of Duisburg-Essen, 45141, Essen, Germany.

[3] Research Unit for Comparative Microbiome Analysis, Helmholtz Zentrum München, 85758, Oberschleißheim, Germany.

To whom the correspondence should be addressed:

alexander.probst@uni-due.de

schulze-makuch@tu-berlin.de

Abstract

The hyperarid core of the Atacama Desert is an extremely harsh environment previously thought to be colonized by only a few heterotrophic bacterial species. In addition, carbon and nitrogen cycling in these highly oligotrophic ecosystems are poorly understood. Here we genomically resolved a novel genus of *Thaumarchaeota, Ca. Nitrosodesertus,* found below boulders of the Atacama hyperarid core, and used comparative genomics to analyze their pangenome and site-specific adaptations. Their genomes contain genes for ammonia oxidation and the 3-hydroxypropionate/4-hydroxybutyrate carbon fixation pathway, indicating a chemolithoautotrophic lifestyle. *Ca. Nitrosodesertus* possesses the capacity for tolerating extensive environmental stress highlighted by the presence of genes against oxidative stress, DNA damage and genes for the formation of biofilms. These features are likely responsible for their dominance in samples with extremely low water content across three different boulder fields and eight different boulders. Genome-specific adaptations of the genomes included the presence of additional genes for UV resistance, heavy metal transporters, multiple types of ATP synthases, and divergent genes for aquaporins. Our results suggest that *Thaumarchaeota* mediate important carbon and nitrogen cycling in the hyperarid core of the Atacama and are part of its continuous and indigenous microbiome.

Introduction

The surface soils in the hyperarid core (1) of the Atacama Desert are hostile environments characterized by extreme desiccation (water content < 1% by weight), high salt content resulting in low water activity, and high UV irradiation (~ 30 $J \cdot m^{-2}$) (2). Scarce amounts of DNA from these soils have been analyzed in previous studies (2–4) revealing sparse microbial communities with low diversity, dominated by *Actinobacteria* and *Firmicutes*. While these previous studies showed that some of these microbes are likely alive and possibly active, as indicated by cultivation experiments (3) and *in-situ* replication measures [iRep; (5)] (2), very little is known about the carbon and nitrogen cycling in the hyperarid soils of the Atacama Desert. To date, only localized carbon fixation could be inferred from the findings of hypolithic and endolithic cyanobacteria (6,7), but no information on possible pathways for the transformation of other nutrients has been obtained so far. A recent study (8) of playas and alluvial fans located outside the hyperarid core reported the presence of Thaumarchaeal 16S rRNA sequences in the subsurface after a heavy rain event (40-90 mm) in 2015. However, without the genome-level information, Thaumarchaeal metabolic capability and contribution to the overall prokaryotic community could not be resolved in this study.

Thaumarchaeota mediate important environmental processes in both marine and terrestrial ecosystems and are particularly adapted to oligotrophic environments with their highly energy-efficient carbon fixation pathway (9,10). *Thaumarchaeota* have also been found in hot desert soils (e.g. Mojave Desert, California and Chihuahuan Desert, New Mexico) (11). However, most in-depth desert microbiome studies focus on bacterial communities (12,13) and multiple studies have reported decreasing archaeal diversity with increasing aridity (14,15). The general pattern of lower

tolerance of *Archaea* to hyperaridity was supported by the absence of *Archaea* in other hyperarid environments such as the McMurdo Dry Valleys, Antarctica (12,16). The soil microbiome of the Atacama Desert has previously been thought to be dominated by *Bacteria*, with an exception of halophilic *Archaea* (*Halobacteriales*) in less arid locations such as coastal soils (2) and salt crusts (17). To our knowledge, previous molecular based studies of the hyperarid core revealed no evidence of *Archaea* and consequently, their adaptations and ecological roles in arid to hyperarid environments have not yet been studied.

The Atacama Desert hyperarid core harbors many expansive boulder fields (18–20) where individual boulders have been exposed for up to 37 millions of years (21,22) and transported by seismic activity. Despite the unique environments that the soils under the boulders present and the ubiquitousness of boulders in the Atacama Desert, no study has determined the microbial and geochemical composition below the boulders. In order to understand these uniquely protected hyperarid soils below the boulders that could harbor microbes playing a key role in carbon and nitrogen cycling in the Atacama Desert, we performed genome-resolved metagenomics of samples from the surface soil below the boulders and compared them to samples beside the boulders. Community structure and metabolic functions were interpreted in conjunction with geochemical measurements. *Thaumarchaeota* were revealed to be one of the key organisms differentiating microbial communities inhabiting below and beside boulders. Consequently, Thaumarchaeal genomes were selected for an in-depth pangenomic analysis to reveal adaptations to environmental stress and potential for carbon and nitrogen cycling. We investigated how *Thaumarchaeota* evolved in these uniquely protected, sparsely populated, and constantly selective environments.

Material and methods

Sampling location and procedure. Sampling was conducted in March 2019, in a dry period with the last recorded rain event occurring in June 2017 in the Yungay region . Three sampling sites, Yungay (Y), Maria Elena (M), and Lomas Bayas (L), were chosen based on a previous study (2) that identified inland hyperarid sites using the threshold of water content <1% by weight (**Figure 1a**). The coordinates of the three sample sites can be found in **Table S1**. Sampling was conducted in previously described characteristic boulder fields (18,19). At each boulder field, six boulders of diameter ~50 cm and height ~20 cm were chosen within a radius of ~100 m from each other. For each boulder, two types of samples were taken, one below boulder (B) and one control sample (C) in the open soil ~10 cm away from the boulder. All chosen boulders were well distanced from other boulders to make sure that the control samples were not constantly shadowed by other boulders or the sampled boulder itself. Samples were taken aseptically using precautions such as wearing a mask and sampling in upwind direction. New gloves were used for each sample, metal spatulas were previously autoclaved in aluminum foil, and newly unfoiled spatulas were used to scoop the topsoil (~0.5 cm) into sterile 50 ml falcon tubes, which were then flash frozen in a liquid nitrogen dry shipper within half an hour of sampling. Control soil samples were taken first and then boulders were flipped over to sample below boulder soil as soon as possible to avoid aerial contamination. Additional samples were taken for geochemical analyses with a small shovel into a PE-sample bag (Whirl-Pak®, WI, USA) which were then stored at room temperature in the dark. See **Supplementary Materials and Methods M1** for additional field measurements.

Geochemical and mineralogical analysis. Detailed methods for pH and electrical conductivity, anion and cation analysis, total organic carbon analysis and bulk mineralogy can be found in the

Supplementary Materials and Methods M2-5.

DNA extraction, Illumina library preparation and sequencing are presented in the **Supplementary Materials and Methods M6**.

Metagenomic analysis, binning and annotation. Out of 24 attempted DNA extractions (**Table S2**, **Figure S1**), 15 yielded measurable amounts of DNA due to extremely low DNA content. Of those, eleven DNA extracts successfully yielded metagenomic libraries and subsequent metagenomic analyses were performed. For detailed methods on assembly, binning and annotation see **Supplementary Materials and Methods M7**.

Community analysis based on metagenomics. Operational taxonomic units (OTUs) were determined by extracting all S3 ribosomal proteins (rPS3) using hmmsearch (HMMER 3.2.1, http://hmmer.org/) across all assembled metagenomes. Retrieved rpS3 amino acid sequences were clustered using USEARCH (23) at 99% identity (24) and centroid sequences were extracted. Coverages of OTUs across all samples were calculated by mapping reads from each sample to the scaffolds of the centroids using Bowtie2 in sensitive mode (25) and filtering for a maximum of 5 mismatches (2% error rate) in both reads in each read pair. Coverages were then normalized by the total number of reads per sample. OTUs were placed into a phylogenetic tree by aligning using MUSCLE (26), alignment trimming using BMGE (BLOSUM30) (27) in default mode, and tree construction using iqtree v1.3.11.1 (28) with flags -m TEST -alrt 1000 -bb 1000. The phylogenetic tree was visualized using iToL (29). Shannon-Wiener Indices were calculated using the Vegan package (30) in R (31). ANOVA (34) analysis was conducted in R (31). Bray-Curtis (32) distance matrices were calculated for Principal coordinate analyses (PCoA), Non-metric multidimensional

scaling (NMDS), BioENV(33), and Multiple response permutation procedures (MRPP, permutation=999) (35), which were subsequently visualized in R (31).

Phylogenomic analysis. Phylogenomic placements of the Thaumarchaeal metagenome-assembled genomes (MAGs) were determined using a supermatrix of 37 single-copy marker genes with all NCBI genomes annotated as *Thaumarchaeota* as of 4/6/2020 (36). The fact that the *Thaumarchaeota* classification on NCBI includes the newly reclassified phylum *Aigarchaeota* (Hua et al. 2018) allowed us to use the latter as an outgroup. CheckM (37) was used to quality filter genomes with thresholds <5% contamination, >50% completeness. Two local databases were created from the Atacama Desert and NCBI Thaumarchaeota MAGs (**Table S13**) respectively, against which homology searches were performed with HMMER 3.2.1 (http://hmmer.org/) using the HMM profiles for the Phylosift marker genes (36) with a cutoff of 1E-5. The resulting datasets were aligned with MUSCLE with default parameters (26) and curated manually to fuse contiguous fragmented sequences and remove extra gene copies. Ultimately, two genomes (GCA_011605725, GCA_011773305) were removed entirely, since they contained multiple sequences that were too distant from both *Thaumarchaeota* and *Aigarchaeota*. The resulting datasets were realigned as above, trimmed with BMGE (BLOSUM30) (27), and concatenated into a supermatrix of 312 operational taxonomic units (OTUs) and 7426 positions. Phylogenies were reconstructed with IQ-TREE 2 (28); first a tree with ModelFinder (38) (-m MFP -bb 1000 -alrt 1000 -abayes) that served as guide tree for a run with the PMSF model (39) (-m LG+C60+F+G -bb 1000 -alrt 1000 -abayes). As per the suggestion of the IQ-TREE authors, we considered those branches strongly supported with at least 95 for ultrafast bootstrap (40) and 80 for the SH-aLRT test (41).

152

153 ***Comparative genomics.*** The predicted protein sequences of eight NCBI *Ca. Nitrosocosmicus*
154 reference genomes (**Table S3**) were compared with the recovered Thaumarchaeal MAGs. The
155 CompareM package (github.com/dparks1134/CompareM) was used to identify the orthologous
156 fraction (OF) and calculate the average amino acid identity (AAI) of orthologous genes between a
157 pair of genomes, and fastANI (42) was used to calculate the average nucleotide identity between
158 genomes using default parameters. OrthoVenn2 (43) was used to identify and visualize
159 orthologous clusters across genomes.

160

161 ***Data availability.*** All sequencing data will be submitted to SRA and genomes will be made
162 publicly available through NCBI.

Results and Discussion

Hyperarid soils sheltered under the boulders are geochemically distinct and organic carbon deficient. As previously documented (18–20,44), a substantial part of the Atacama Desert hyperarid core features expansive boulder fields, where the topsoil is covered by boulder-sized clasts (**Figure. 1, Figure S4**). Soils below the boulders experience lower diurnal temperature and relative humidity fluctuations than soils beside the boulders (**Figure S2a-c**). Based on the dew point temperature calculations, we showed that the condensation of water in the morning hours is far less likely for soil below boulders compared to soil beside boulders (**Figure S2d-f**), suggesting that water content below boulders may be even lower than previously studied Atacama Desert hyperarid top soils (~0.2% by weight) (2).

We compared soil samples of two sample types: soils taken below boulders (B) and soils taken adjacent to the boulder (control, C), at three different sampling locations (Lomas Bayas, L; Maria Elena, M; Yungay Valley, Y) (**Figure 1a**). While the collected soils were mineralogically very similar with some variation with sampling location (**Figure S3**), their ion concentrations showed large variance between boulder fields, individual boulders, and sample types. Interestingly, B samples clustered based on their sampling location, while C clustered independent of sampling sites (**Figure 1b)**. In general, samples from locations L and M were enriched in F^-, while Y samples were enriched in PO_4^{3-}, SO_4^{2-}, Mn^{2+} and Ca^{2+}, suggesting boulder field specific patterns of ion concentrations. More sampling location dependent ion composition patterns amongst the B samples indicate that soils below the boulder are sheltered from external input of ion species (i.e. atmospheric deposition), thereby exhibiting a more representative ion composition patterns of the soils in the area beyond the topsoil. When comparing the B and C sample of each individual boulder, nitrate and magnesium ion concentrations were significantly lower in B samples compared to C samples (paired t-test; NO_3^-: $t(8) = -3.9$, p-value = 0.0451, Mg^{2+}: $t(8) = -$

2.33, p-value = 0.0484, **Figure S5**). Total Organic Carbon (TOC) concentrations were at or below detectable levels (**Figure S6**) in both below boulder and beside boulder samples. Our results show that the soils below the boulders are not only hyperarid and organic carbon deficient, but also sheltered from the atmospheric input of both water (e.g. fog, dew) and ion species.

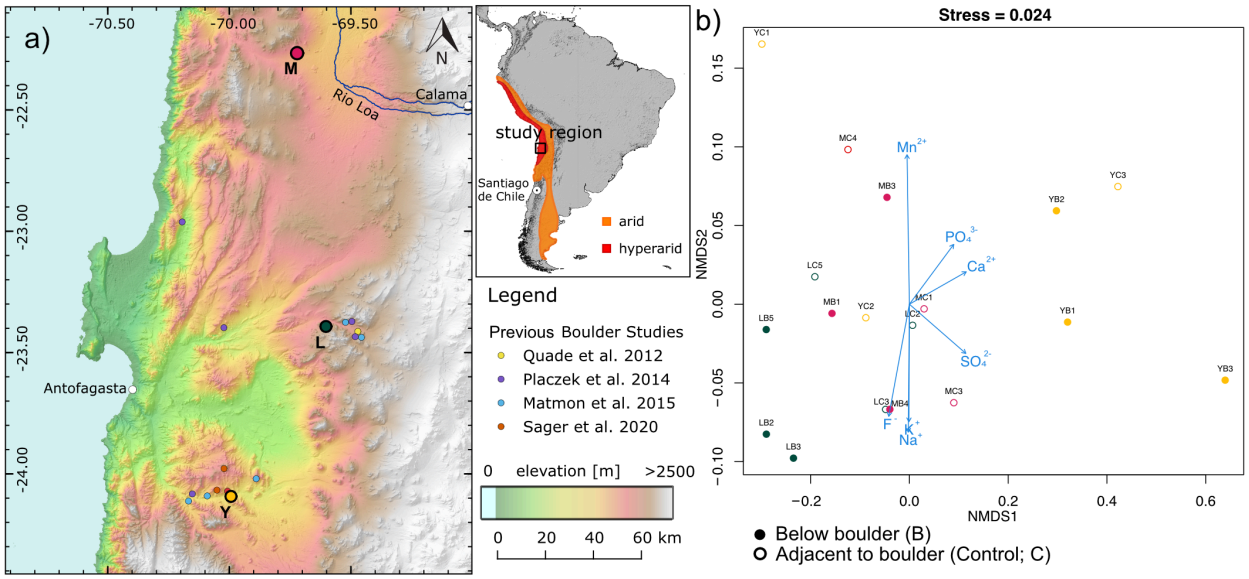

Figure 1. Sampling location and soil geochemistry. a) Location of three sampling sites and their abbreviations in parentheses b) Non-metric multidimensional scaling (NMDS) ordination of anion and cation concentrations in each soil sample. Different colors represent different sampling sites (Green = L, Red = M, Yellow = Y). Filled vs unfilled data points correspond to the sample type information. Blue vectors represent fitted ion species onto the ordination with a p-value less than 0.1.

198

199 ***An actively replicating microbial community in the Atacama Desert hyperarid core.*** We
200 investigated the eleven successfully prepared metagenomes (for details see Material and Methods
201 and **Table S4**): three below boulder and three control samples came from Lomas Bayas (LB2,
202 LB3, LB5 and LC2, LC3, LC5), three samples below boulder were from Maria Elena (MB1, MB3,
203 MB4) and two below boulder samples from Yungay Valley (YB1, YB3).

204 Genome-resolved metagenomics of these eleven samples yielded 73 high quality (>75%
205 completeness, <15% contamination) metagenome-assembled genomes (MAGs), of which 71
206 belonged to only three different phyla, reflecting the limited diversity of this extreme ecosystem.
207 Eight of these high quality genomes were Thaumarchaeal with completeness ranging from 84.67
208 to 98.54% and contamination below 10% (**Table S4**). Other high quality MAGs belonged to
209 *Actinobacteria* (n=34), *Chloroflexi* (n=29), *Firmicutes* (n=1), *Alphaproteobacteria* (n=1). *In situ*
210 replication measures [iRep, (5)] were successfully calculated for 32 out of all high-quality bacterial
211 genomes (n=65), indicating an active metabolism of the majority of the indexed population
212 (calculated iRep values of 32 genomes ranged between 1.34 and 3.47, mean: 1.98). On average,
213 genomes recovered from below boulder metagenomes were associated with higher iRep values
214 than the control metagenomes (p-value < 0.04, Welch's t-test, **Figure S7)**. A full overview of
215 genome statistics, their taxonomic classification and corresponding iRep values is provided in
216 **Table S4**.

217

218 ***Atacama soils below boulders harbor unique microbial communities with high shares of***
219 ***Thaumarchaeota.*** We detected 147 different *Bacteria* and *Archaea* based on clustering of S3
220 ribosomal proteins (rpS3, 99% identity, **Table S5, Figure S8**). Shannon indices showed higher
221 variation in alpha diversity for below boulder samples compared to control samples (**Figure S9**).

Principal Coordinate Analysis (PCoA) of the communities (**Figure S10a**) demonstrated clustering of samples based on the sample site (L, M, Y) as well as the sample type (B, C). This was corroborated by the Multiple Response Permutation Procedure (MRPP) indicating significant influence on the community structure by both sampling location (chance corrected within group agreement A = 0.2648, significance of delta = 0.001) and sample type (A = 0.1488, significance of delta = 0.002). Using BioENV (33), we identified F^- concentration to be most correlated (correlation = 0.573) with the community composition. Additionally, we conducted a NMDS analysis (**Figure S10b**), identifying additional ions (Ca^{2+}, SO_4^{2-}, K^+, Cl^-) that could be correlated with the community composition.

Out of the 147 different taxa, 33 were identified to be significantly different in their abundances (ANOVA (34) p-value < 0.05) between B and C samples (**Table S6**). Such taxa included *Actinobacteria* (belonging to *Cryptosporangiaceae, Streptomycetaceae,* and *Geodermatophilacaea*), as well as one *Alphaproteobacteria* (*Acetobacteraceae*). These taxa were particularly abundant in control samples and near absent in below boulder samples, suggesting specific and unknown selection processes for the two different sample types. Alternatively, some of these taxa may be deposited through aeolian transport (45)**. Figure 2** shows the phylogenetic relationship between the top 30 most abundant taxa across the samples based on rpS3 proteins and links them to their respective MAGs as well as their differential coverage across the samples. We conclude that below boulder (B) and beside boulder (C) present substantially different habitats of the same ecosystem.

One *Thaumarchaeal* OTU was the only taxon based on ANOVA (34) (p-value = 0.0396) with a higher abundance below boulders and near absence in control samples. All eight below boulder metagenomes contained high abundances of *Thaumarchaeota*. Based on the ranked

abundance of ribosomal protein S3 (rpS3) gene coverages, *Thaumarchaeota* ranked amongst the top seven most abundant taxa across all below boulder samples. In three samples (MB3, MB4, LB5), *Thaumarchaeota* were the most abundant organisms, e.g. in LB5, *Thaumarchaeota* were 4-fold more abundant than the second most abundant taxon. The abundance of *Thaumarchaeota* under boulders and their near absence in the nearby irradiated soil support the previous findings from marine environments (10,46) where surface waters harbored lower abundances of *Thaumarchaeota*. Photoinhibition of ammonia oxidation in ammonia oxidizing archaea (AOA) (47) has previously been hypothesized as the cause, along with other proposed hypotheses, such as increased competition (48,49) and indirect photoinhibition by Reactive Oxygen Species (ROS), such as hydrogen peroxide (50). To date, the underlying reason for the lower abundance of *Thaumarchaeota* in highly irradiated environments remains inconclusive. Based on the low amounts of DNA recovered from most control samples (< 1.14 ng / g soil), we conclude that the near absence of *Thaumarchaeota* in the open irradiated top soils is likely not due to increased competition, at least at our study sites. Photochemically produced ROS (H_2O_2 and metal superoxides and peroxides) have previously been found to accumulate in the Atacama Desert (Yungay site) top soils at levels an order of magnitude higher than in non-arid control soils (51). Additionally, in contrast to ocean environments, UV and photoradiation do not penetrate into the soil beyond the very surface of the topsoil and with minimal soil turbation in the Atacama, we expect the effect of UV and photoradiation inhibition reaching below the top ~ 0.5 cm of soil unlikely. Therefore, we hypothesize the inhibition of high ROS levels (50) to be the main reason why *Thaumarchaeota* are not abundant in the control samples despite their potential desiccation tolerance.

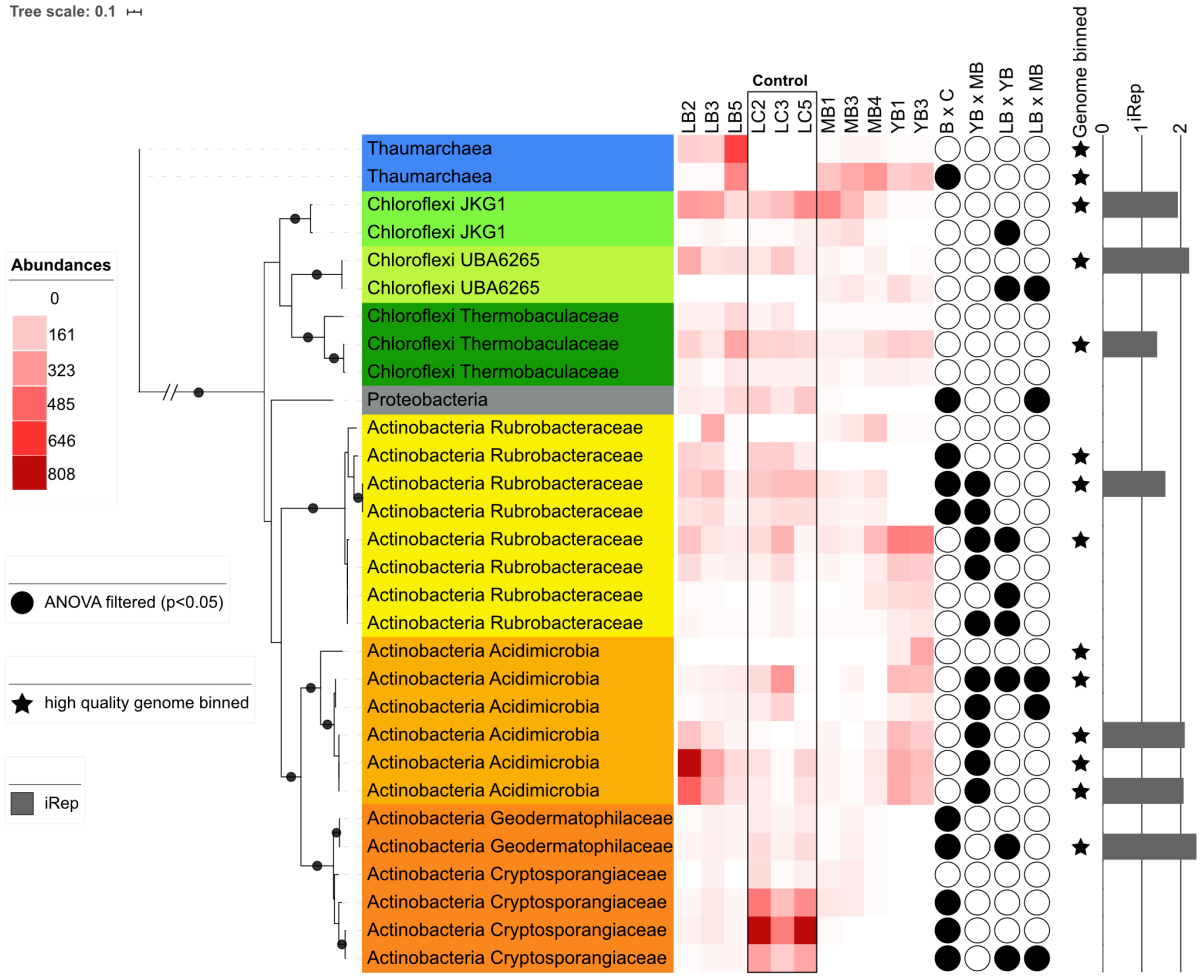

Figure 2. Phylogenetic tree of 30 most abundant taxa (rps3 clusters) out of 147 and their normalized abundances across all samples. Filled stars represent successful binning of the OTU in high quality genomes and red bars indicate iRep values calculated for the high quality genomes. Strongly supported branches as described in the M&M section are indicated with black dots.

Ammonia Oxidizing Thaumarchaeota occupy an important niche in the Atacama Desert carbon and nitrogen cycling. Normalized abundance of key marker genes in the assembled metagenomes revealed potential for C1 metabolism (**Figure 3, Table S7-8**), complex carbon degradation, and fermentation across all samples. Three carbon fixation pathways (3-hydroxypropionate cycle, 3HP/4HB, CBB cycle) were detected however, abundances of each marker gene varied with site. No 3HP/4HB cycle was found in control samples, while the 3-hydroxypropionate cycle was found in low abundance in MB and YB samples. Significant gaps in the potential for nitrogen cycling were observed. Nitrile hydratases were found across all samples, and archaeal ammonia oxidation potential was only found in below boulder samples (with the exception of YB1). No potential for nitrogen fixation, nitrate-, and nitric oxide reduction as well as nitrite oxidation were identified. The lack of nitrogen fixation and denitrification genes suggest low overall biological input and little loss of biologically available nitrogen. Although the investigated soils are known to be enriched in nitrates (particularly at ~1m depth) that have accumulated over millions of years through abiotic processes (e.g. atmospheric formation through lightning followed by dry deposition and rainwater infiltration) (52), below boulder nitrate concentrations are significantly lower (**Figure S5**), likely due a combined effects of highly microbial activity and lack of atmospheric or hydrologic input. Therefore, we propose that nitrogen cycling below boulders is largely controlled by microbial activity. Specifically, we suggest a highly equilibrated nitrogen cycle with *Thaumarchaeota* nitrifying ammonia produced through protein ammonification performed by diverse *Chloroflexi* and *Actinobacteria* (**Table S9**) in these below boulder environments.

Resolving the metabolic potential at the genomic level delineated the role each taxonomic group plays in this highly streamlined community. Presence and absence of key metabolic genes

297 for each high quality genome are shown in **Figure 3b**. Our analysis shows that although all samples
298 show carbon fixation potential, taxa capable of fixing carbon are limited to *Thaumarchaeota*
299 (through the 3HP/4HB pathway) and some *Rubrobacteraceae* (3-hydroxypropionate pathway).
300 Surprisingly, only one Form I Rubisco could be binned to a high quality *Rubrobacteraceae*
301 genome, despite a stronger signal seen in the metagenomes. Chloroflexi genomes associated with
302 the lineage *JKG1* had the broadest potential of degrading complex carbon and were capable of a
303 fermentative lifestyle, while *Actinobacteria* could metabolize a wider range of C1 substrates.
304 Nitrite reduction potential detected in below boulder sites was constrained to the nirK genes found
305 in *Thaumarchaeota*. NirK in *Thaumarchaeota* has been hypothesized to play a key role in
306 ammonia oxidation (53), and is biochemically capable of transforming N compounds to produce
307 nitric oxide (54). However, whether it also denitrifies organic nitrite leading to a loss of organic N
308 in a natural environment remains to be confirmed. Genome-resolved metabolic predictions
309 revealed conserved metabolic capacities across genomes that belong in the same taxonomic family,
310 with *Thaumarchaeota* playing a unique role in the nitrogen and carbon cycling in the Atacama
311 hyperarid core.

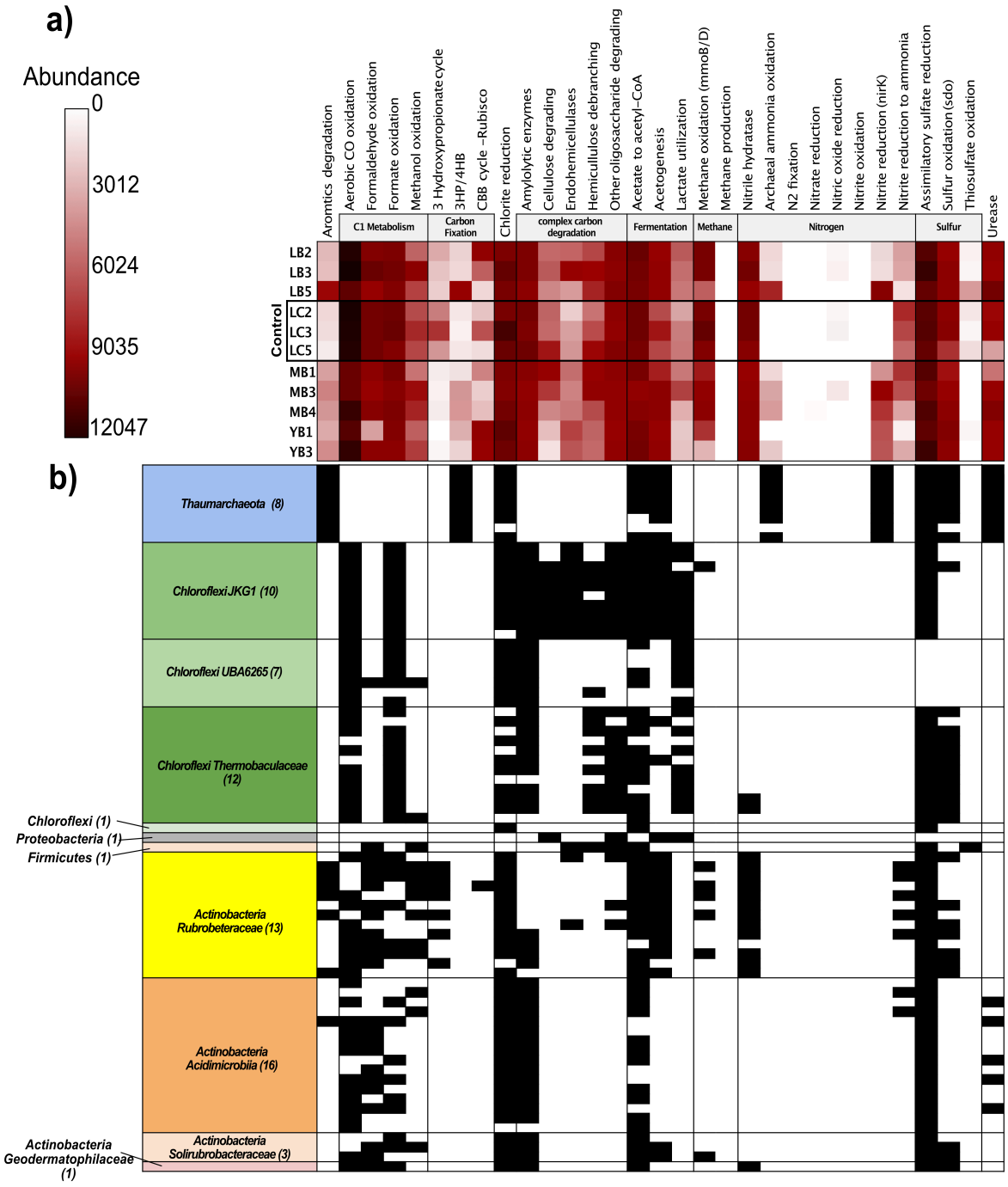

Figure 3. Metabolic potential prediction across samples and high quality genomes. a) Normalized abundances of chemoautolithotrophic marker genes predicted using METABOLIC for each sample. b) Presence (black) and absence (white) of chemoautolithotropic marker genes in

316 high quality genomes. Genomes are clustered based on taxa and the number of genomes in each
317 cluster is shown in parentheses in the row names.
318
319 ***A novel genus of Thaumarchaeota with highly conserved core genome and diverse auxiliary***
320 ***genes.*** Eight high quality Atacama Boulder Thaumarchaeal genomes (ABT) were assembled with
321 an average GC content of 34.6% (± 0.1%) and average size of 2.5 Mbps (± 0.4 Mbps). Each
322 genome contained on average 3,123 (± 579.7) predicted genes with a mean coding density of
323 71.8% (± 1.7%). The genomes were phylogenetically placed using 37 single-copy house-keeping
324 genes, forming a monophyletic sister cluster to the recently characterized *Ca. Nitrosocosmicus*
325 (**Figure 4a**). The ABT clade and *Ca. Nitrosocosmici* form a sister group to *Ca. Nitrososphaera*, a
326 mesophilic terrestrial clade. Genomes from the same sites were more related to each other, with
327 ABT-MB and ABT-YB genomes forming a separate branch from the ABT-LB genomes (**Figure**
328 **4b**). One copy of the ammonia monooxygenase A (*amoA*) gene was found in five ABT genomes
329 (**Table S10**). Upon closer look, two other genomes (ABT-MB3, ABT-MB4) contained conserved
330 *amoA* regions with unresolved assembly errors and therefore failed in protein prediction. No *amoA*
331 sequences were found in ABT-YB1. 3 additional unbinned *amoA* genes were detected across the
332 metagenomes (MB3, MB4, YB3). Altogether, the eight *amoA* nucleotide sequences were 100%
333 identical in their amino acid sequences to each other and to previously published *amoA* sequences
334 from *Ca. Nitrosocosmicus oleophilus* and *Ca. Nitrosocosmicus exaquare*, which had been
335 phylogenetically identified to be one of the basal clades of archaeal *amoA* after *Ca. Nitrosocaldus*
336 *(55)*. **Figure S11** resolves the nucleotide level phylogenetic placement of binned *amoA* sequences
337 as well as unbinned *amoA* sequences recovered from the sample metagenomes. Interestingly, one
338 *amoA* recovered from a low quality bin (68% completeness; 5.8% contamination) in the YB3
339 metagenome (node "ABT-YB3 (low quality bin)" in **fig. S11**) was divergent (~80% ID) from the

rest at the nucleotide level, while 95.8% identical to other ABT and *Ca. Nitrosocosmicus amoA* genes at the amino acid level. The rpS3 gene recovered from this bin was classified as Thaumarchaeal, with 75% identity to other binned rpS3 in ABT, and its closest NCBI reference sequence being *Ca. Nitrosocosmicus* sequences at 65% identity. This divergent Thaumarchaeal bin was approximately three-fold less abundant than another Thaumarchaeal bin (ABT-YB3) recovered at a higher quality from the same metagenome (YB3). Due to low quality and lower abundance of this divergent bin, our study focuses on other eight high quality genomes that are much more closely related and found across all metagenomes under the boulder including YB3.

In order to taxonomically resolve the eight recovered *Thaumarchaeota* genomes, we compared them to *Ca. Nitrosocosmicus* genomes that had been isolated or metagenomically assembled from around the world (**Table S4**) in diverse environments ranging from the arctic soil (56), tar-contaminated soil (57), vegetable field (58), dinosaur fossil (59) to wastewater filters (60). High ANI (93.0 - 99.8%) (**Figure 4c**) between ABT genomes indicated that all ABT genomes belong to one genus. Using the ANI threshold of 95% (61,62) for species delineation, we identified two species within the ABT clade, with genomes recovered from LB site belonging to one species and the rest to another. The mean Amino Acid Identity (AAI) of 53.9% between pairs of *Ca. Nitrosocosmicus* and ABT genomes (**Figure 4d**) fall below the genus delineation threshold of 65% (63) indicating that the two clades form separate genera. Based on these findings, we propose two new species names that belong to a new genus: *Ca. Nitrosodesertus atacamaensis* (ABT-LB2, ABT-LB3, ABT-LB) and *Ca. Nitrosodesertus subpetramus* (ABT-MB1, ABT-MB3, ABT-MB4, ABT-YB1, ABT-YB3).

While the eight ABT genomes share a highly conserved core genome (mean AAI = 96.5 %), between 11% and 49% (mean = 37.7%) of the genes had no other orthologs in the

363 recovered genomes despite the relatively similar and static environmental conditions that they
364 were found in. High AAI in the orthologous fraction of the eight ABT genomes and conserved
365 *amoA*s recovered in sites more than 200 km apart from each other suggest that ABTs originated
366 from the same strain of *Thaumarchaeota*. However, large fractions of sample-specific auxiliary
367 and divergent genes suggest site-specific adaptations to their respective isolated habitats.

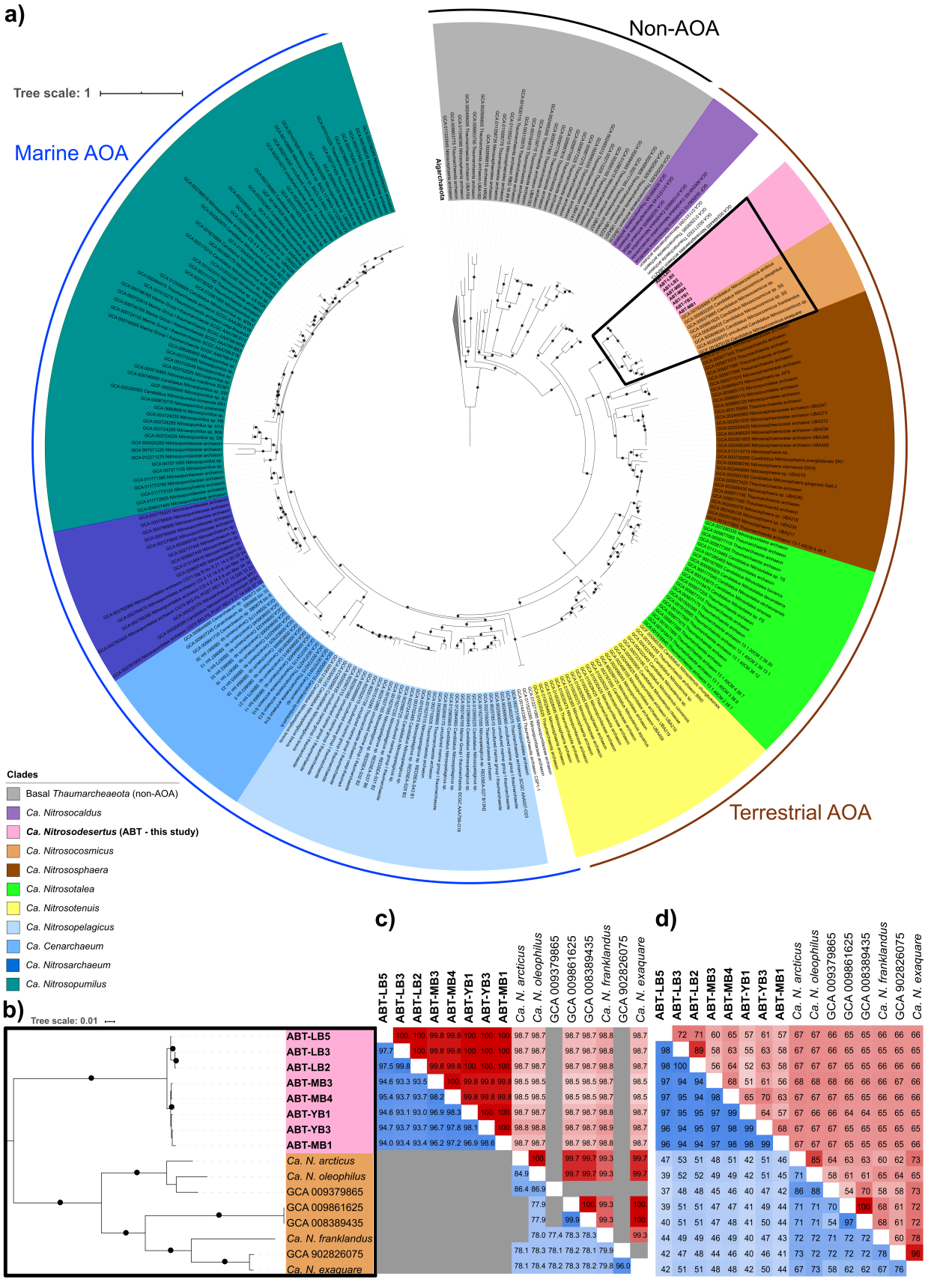

Figure 4. Phylogenomic placement of ABT genomes using 37 housekeeping single-copy genes. a) Phylogenetic tree of 298 NCBI genomes annotated as *Thaumarchaeota* and 8 ABT genomes. *Aigarchaeota* were identified and used as the outgroup. Black, brown and blue ranges distinguish whether organisms are Ammonia Oxidizing Archaea (AOA) and their typical habitats (terrestrial vs marine). Strongly supported branches as described in the M&M section are indicated with black dots. b) Zoomed view of the branches placing the ABT genomes and its sister group *Ca. Nitrosocosmicus.* Strongly supported branches as described in the M&M section are indicated with black dots. c) Lower-right (blue) triangle of the matrix corresponds to FastANI between genomes, where gray values indicate below calculation threshold (80% identity). Upper right (red) triangle of the matrix corresponds to 16S rRNA identity values, where gray values are used for genomic bins without a 16S rRNA. d) Lower right (blue) triangle corresponds to the Amino Acid Identity (AAI) and upper right (red) triangle corresponds to the Orthologous fraction (OF) between a pair of compared genomes.

Pangenomic comparison of ABT genomes and their sister clade reveal unique adaptations including heavy metal resistance, biofilm formation, water transport and sodium bioenergetics.

In order to understand the conserved metabolic potentials between ABT and *Ca. Nitrosocosmicus*, unique adaptations of the ABT in the Atacama Desert, and niche differentiations between sites, we analyzed the highest quality (> 95% completeness, <5% contamination) genomes (ABT-LB3, ABT-MB4, ABT-YB3) from each of the three sites along with three (near)-complete *Ca. Nitrosocosmicus* reference genomes (*Ca. N. franklandus, Ca. N. oleophilus, Ca. N.exaquare*). 1287 homolog clusters are shared across all six genomes (**Figure 5**, **Table S10**). For example, all genomes contained a highly conserved AmoABX operon, although only two out of eight ABT bins contained 1-2 *amoC* copies. All genomes revealed the metabolic potential for mixotrophy along with important genes for nitrogen cycling, including genes for copper-dependent nitrite reductase (*nirK*), urease (*Ure*), urea transporter, ammonium transporter, deaminases, lyases, and carbonic anhydrase (**Table S11**). Additionally, amongst the shared genes we found key stress response genes that could provide resilience against highly oxidizing environments (**Table S10**).

296 protein clusters were shared between ABT genomes but were not present in *Ca. Nitrosocosmicus* genomes (**Figure 5)**. Notable genes identified in these clusters include those involved in biofilm production and cell adhesion capacity (**Table S10**). The ability of Ca. *Nitrosocosmicus oleophilus* to form biofilms and produce exopolysaccharide (EPS) has previously been demonstrated by Jung *et al.* (57). EPS production and biofilm formation in general are considered major adaptation mechanisms for xerotolerant bacteria (64) and ABT genomes may also employ this mechanism to protect against desiccation.

12.8% to 16.5% of the protein coding genes in each ABT genome belonged to unique protein clusters or were singletons (**Figure 5, Table S12)** that did not share any similarity to other

genes in the ABT genomes. Amongst singletons of the genome ABT-LB3, many were involved in membrane transport of metals, such as magnesium, copper and cobalt transporters as well as lead, cadmium, zinc and mercury transporting ATPases, potassium uptake proteins and bacterioferritin. The presence of these genes may be an adaptation to heavy metals known to accumulate in the Atacama Desert soils (65). Similarly, notable singletons found in genomes ABT-MB4 and ABT-YB3 included putative cobalt transporter, fluoride transporters, zinc uptake system, mercuric reductase, ferrous iron permease, and phosphite transport system. See supplementary results for further findings from the pangenome analysis.

Further genome comparisons across all eight ABT genomes revealed additional key adaptations to desiccation and osmotic stress. We identified up to seven different copies of water channel membrane proteins (aquaporin Z2) (66) per genome. Interestingly, some of these proteins were highly divergent from each other at the AA sequence level, while others were truncated (**Figure S12**) despite being found mid-contig with relatively conserved surrounding genes. Multiple copies of aquaporin genes per genome as well as the divergent and truncated subset indicate possible genome specific adaptations to desiccation and osmotic stress. We also recovered two distinct types of ATP synthases (namely A-type and V-type (67,68)) from the eight ABT genomes. Three ABT genomes (ABT-LB2, ABT-LB3, ABT-YB1) contained only A-type ATP synthase, while the rest contained both the A-type and the V-type ATP synthases often in multiple copies. Wang *et al.* (67) concluded that the V-type ATP synthases are horizontally transferred from *Euryarchaeota* and conserved among the acidophilic and hadopelagic *Thaumarchaeota*, potentially playing a key role in adaptations to acidic environments and elevated pressure through proton extrusion. Considering that Atacama Desert soils are slightly alkaline (average pH = 7.7 **Figure S13**), it is surprising that the V-type ATP synthase is found and conserved across five ABT

genomes. Zhong *et al*. (68) hypothesized that these V-type ATP synthases may be coupled with Na^+ motive force instead of proton pumping. Atacama Desert soils present high salt stress, and therefore the V-type ATP synthase could perform Na^+ pumping and provide protection against high sodium stress (**Table S14**). Notably, all genomes featured high-affinity Na^+/H^+ antiporter NhaS, with ABT-LB2 and ABT-LB3 genomes featuring five copies, while the others featured a single copy. This may be correlated to the lack of Na^+ binding V-type ATP synthase in ABT-LB2 and ABT-LB3 genomes. Additional genes associated with Na^+ bioenergetics were identified, including sodium/glucose transporter, putative calcium/sodium:proton antiporter, sodium bile acid symporter family protein, sodium/hydrogen exchanger and sodium-dependent dicarboxylate transporters. This suggests that ABT genomes are not only highly adapted to high salt concentrations but also are potentially capable of utilizing the sodium gradient to scavenge useful biomolecules for mixotrophic growth as well as generate ATP in the hyperarid core of the Atacama Desert.

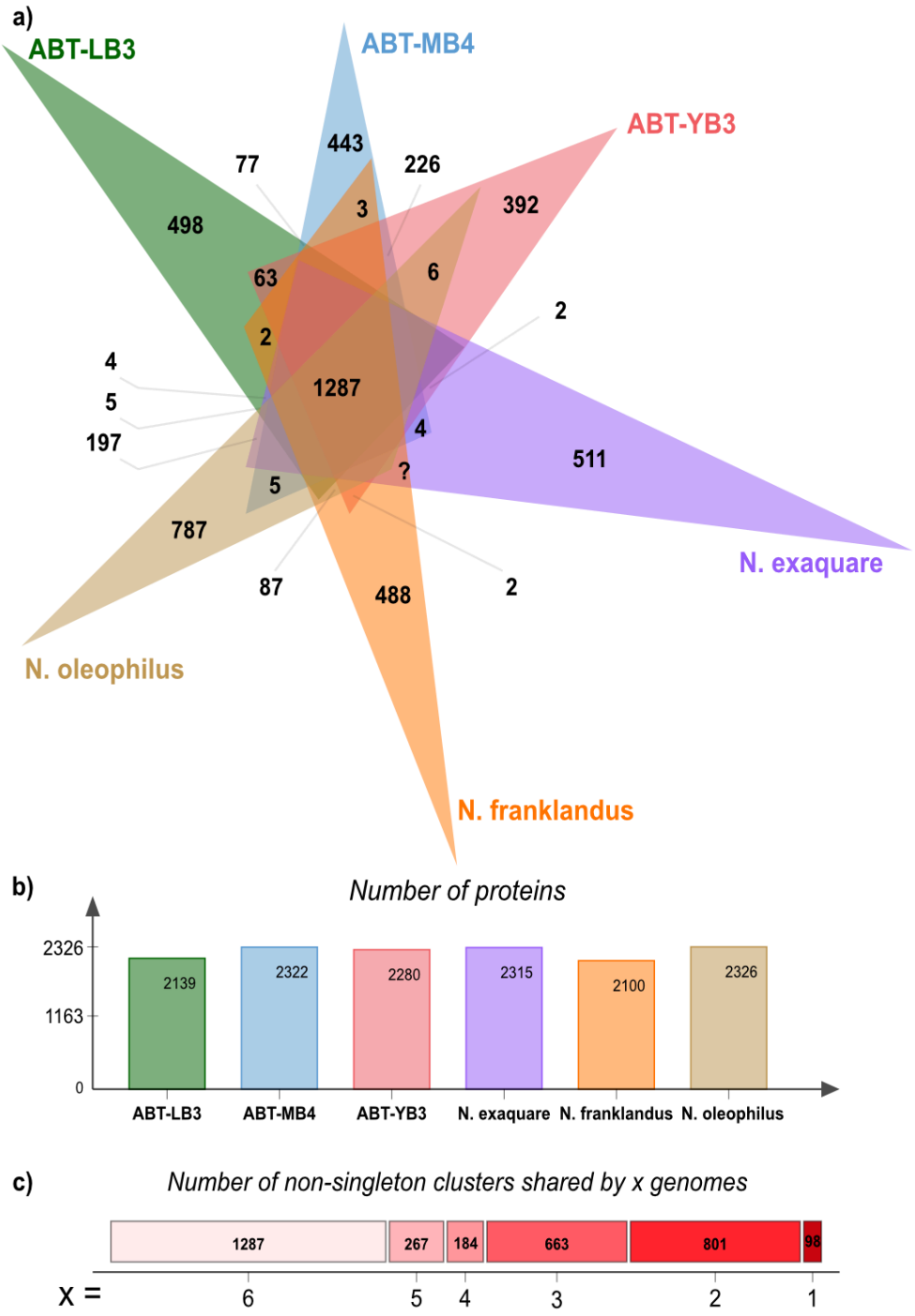

Figure 5. Shared and auxiliary protein clusters of ABT and its sister genus. a) Shared orthologous protein clusters (including singletons) across six genomes (three Ca. *Nitrosocosmicus*, three Ca. *Nitrosodesertus* [ABT]). b) Number of proteins in each genome. c) Number of orthologous protein clusters (excluding singletons) shared across x number of genomes.

Conclusions

We report here the first evidence of highly adapted ammonia-oxidizing *Thaumarchaeota* inhabiting the hyperarid Atacama Desert in high relative abundance, including the first systematic comparison of microbial communities found below boulders of the Atacama Desert hyperarid core with the microbial communities present in the open, unprotected desert soil. This study expands the realm of Thaumarchaeal presence revealing high adaptability and resilience to hyperarid, high salt and low-nutrient environments. In-depth genomic characterization of these ABT genomes elucidated their niche potential roles in N and C cycling in highly nutrient deficient Atacama Desert soils, as well as key adaptations against oxidative stress, salt stress and hyperaridity. By comparing the eight closely related ABT genomes retrieved from these isolated and disconnected habitats, we hypothesize *Ca. Nitrosodesertus* to be a potentially endemic *Thaumarchaeota* genus in the Atacama Desert, with organisms in this genus harboring highly conserved shared genes and large numbers of site-specific auxiliary genes. Beyond the Atacama Desert, this study provides a blueprint for future studies of extreme terrestrial environments (i.e. Antarctic and extraterrestrial) where finding pockets of pristine, sheltered and contained environments, as simple as below boulders, could lead to a discovery of uniquely conserved communities and help delineate the indigenous microbial community members adapted to extreme conditions.

Acknowledgements

This work was funded by ERC Advanced Grant HOME (# 339231) to DSM. AJP and TVLB were supported by the Ministerium für Kultur und Wissenschaft des Landes Nordrhein-Westfalen ("Nachwuchsgruppe Dr. Alexander Probst"). We thank Bärbel Försel for insightful discussions, Manuela Alt and Kirstin Weiß for TOC measurements, Thomas Neumann for providing access to the XRD laboratory, and Iris Pieper and Claudia Kuntz for technical assistance and measurement of water-soluble ion species.

Competing Interests

All authors declare that they have no competing interests.

Author contributions

DSM and YH conceived the project; YH, FLA, and AA planned and conducted sampling; JSS and MS prepared metagenomic libraries and performed sequencing as well as initial quality filtering of reads; YH assembled, curated and analyzed sequence data with contribution from TLVB and AJP; AJP provided computational resources; FLA performed geochemical analyses and AA provided input in data interpretation; PSA performed phylogenetic analysis; YH wrote the manuscript with contribution from AJP; all authors discussed and revised the manuscript.

References

1. Houston J, Hartley AJ. The central Andean west-slope rainshadow and its potential contribution to the origin of hyper-aridity in the Atacama Desert [Internet]. Vol. 23, International Journal of Climatology. 2003. p. 1453–64. Available from: http://dx.doi.org/10.1002/joc.938

2. Schulze-Makuch D, Wagner D, Kounaves SP, Mangelsdorf K, Devine KG, de Vera J-P, et al. Transitory microbial habitat in the hyperarid Atacama Desert. Proc Natl Acad Sci U S A. 2018 Mar 13;115(11):2670–5.

3. Azua-Bustos A, Caro-Lara L, Vicuña R. Discovery and microbial content of the driest site of the hyperarid Atacama Desert, Chile [Internet]. Vol. 7, Environmental Microbiology Reports. 2015. p. 388–94. Available from: http://dx.doi.org/10.1111/1758-2229.12261

4. Navarro-González R, Rainey FA, Molina P, Bagaley DR, Hollen BJ, de la Rosa J, et al. Mars-like soils in the Atacama Desert, Chile, and the dry limit of microbial life. Science. 2003 Nov 7;302(5647):1018–21.

5. Brown CT, Olm MR, Thomas BC, Banfield JF. Measurement of bacterial replication rates in microbial communities [Internet]. Vol. 34, Nature Biotechnology. 2016. p. 1256–63. Available from: http://dx.doi.org/10.1038/nbt.3704

6. Azúa-Bustos A, González-Silva C, Mancilla RA, Salas L, Gómez-Silva B, McKay CP, et al. Hypolithic Cyanobacteria Supported Mainly by Fog in the Coastal Range of the Atacama Desert [Internet]. Vol. 61, Microbial Ecology. 2011. p. 568–81. Available from: http://dx.doi.org/10.1007/s00248-010-9784-5

7. Moreno ML, Piubeli F, Bonfa MRL, García MT, Durrant LR, Mellado E. Analysis and characterization of cultivable extremophilic hydrolytic bacterial community in heavy-metal-contaminated soils from the A tacama D esert and their biotechnological potentials. J Appl Microbiol. 2012;113(3):550–9.

8. Fernández-Martínez MÁ, Dos Santos Severino R, Moreno-Paz M, Gallardo-Carreño I, Blanco Y, Warren-Rhodes K, et al. Prokaryotic Community Structure and Metabolisms in Shallow Subsurface of Atacama Desert Playas and Alluvial Fans After Heavy Rains: Repairing and Preparing for Next Dry Period. Front Microbiol. 2019 Jul 24;10:1641.

9. Könneke M, Schubert DM, Brown PC, Hügler M, Standfest S, Schwander T, et al. Ammonia-oxidizing archaea use the most energy-efficient aerobic pathway for CO2 fixation. Proc Natl Acad Sci U S A. 2014 Jun 3;111(22):8239–44.

10. Karner MB, DeLong EF, Karl DM. Archaeal dominance in the mesopelagic zone of the Pacific Ocean. Nature. 2001 Jan 25;409(6819):507–10.

11. Fierer N, Leff JW, Adams BJ, Nielsen UN, Bates ST, Lauber CL, et al. Cross-biome metagenomic analyses of soil microbial communities and their functional attributes. Proc Natl Acad Sci U S A. 2012 Dec 26;109(52):21390–5.

12. Pointing SB, Chan Y, Lacap DC, Lau MCY, Jurgens JA, Farrell RL. Highly specialized microbial diversity in hyper-arid polar desert. Proc Natl Acad Sci U S A. 2009 Nov 24;106(47):19964–9.

13. Maza F, Maldonado J, Vásquez-Dean J, Mandakovic D, Gaete A, Cambiazo V, et al. Soil Bacterial Communities From the Chilean Andean Highlands: Taxonomic Composition and Culturability. Front Bioeng Biotechnol. 2019 Feb 5;7:10.

14. Neilson JW, Califf K, Cardona C, Copeland A, van Treuren W, Josephson KL, et al. Significant Impacts of Increasing Aridity on the Arid Soil Microbiome. mSystems [Internet]. 2017 May;2(3). Available from: http://dx.doi.org/10.1128/mSystems.00195-16

15. Huang M, Chai L, Jiang D, Zhang M, Zhao Y, Huang Y. Increasing aridity affects soil archaeal communities by mediating soil niches in semi-arid regions. Sci Total Environ. 2019 Jan 10;647:699–707.

16. Singh BK. Archaea in a hyper-arid polar desert [Internet]. Vol. 107, Proceedings of the National Academy of Sciences. 2010. p. E1–E1. Available from: http://dx.doi.org/10.1073/pnas.0912316107

17. Finstad KM, Probst AJ, Thomas BC, Andersen GL, Demergasso C, Echeverría A, et al. Microbial Community Structure and the Persistence of Cyanobacterial Populations in Salt Crusts of the Hyperarid Atacama Desert from Genome-Resolved Metagenomics. Front Microbiol. 2017;8:1435.

18. Matmon A, Quade J, Placzek C, Fink D, Copeland A, Neilson JW, et al. Seismic origin of the Atacama Desert boulder fields [Internet]. Vol. 231, Geomorphology. 2015. p. 28–39. Available from: http://dx.doi.org/10.1016/j.geomorph.2014.11.008

19. Quade J, Reiners P, Placzek C, Matmon A, Pepper M, Ojha L, et al. Seismicity and the strange rubbing boulders of the Atacama desert, Northern Chile. Geology. 2012 Sep 1;40(9):851–4.

20. Sager C, Airo A, Arens FL, Rabethge C, Schulze-Makuch D. New types of boulder accumulations in the hyper-arid Atacama Desert [Internet]. Vol. 350, Geomorphology. 2020. p. 106897. Available from: http://dx.doi.org/10.1016/j.geomorph.2019.106897

21. Placzek CJ, Matmon A, Granger DE, Quade J, Niedermann S. Evidence for active landscape evolution in the hyperarid Atacama from multiple terrestrial cosmogenic nuclides. Earth Planet Sci Lett. 2010 Jun 15;295(1):12–20.

22. Dunai TJ, González López GA, Juez-Larré J. Oligocene–Miocene age of aridity in the Atacama Desert revealed by exposure dating of erosion-sensitive landforms [Internet]. Vol. 33, Geology. 2005. p. 321. Available from: http://dx.doi.org/10.1130/g21184.1

23. Edgar RC. Search and clustering orders of magnitude faster than BLAST. Bioinformatics. 2010 Oct 1;26(19):2460–1.

24. Sharon I, Morowitz MJ, Thomas BC, Costello EK, Relman DA, Banfield JF. Time series

community genomics analysis reveals rapid shifts in bacterial species, strains, and phage during infant gut colonization. Genome Res. 2013 Jan;23(1):111–20.

25. Langdon WB. Performance of genetic programming optimised Bowtie2 on genome comparison and analytic testing (GCAT) benchmarks. BioData Min. 2015 Jan 8;8(1):1.

26. Edgar RC. MUSCLE: a multiple sequence alignment method with reduced time and space complexity. BMC Bioinformatics. 2004 Aug 19;5:113.

27. Criscuolo A, Gribaldo S. BMGE (Block Mapping and Gathering with Entropy): a new software for selection of phylogenetic informative regions from multiple sequence alignments [Internet]. Vol. 10, BMC Evolutionary Biology. 2010. p. 210. Available from: http://dx.doi.org/10.1186/1471-2148-10-210

28. Nguyen L-T, Schmidt HA, von Haeseler A, Minh BQ. IQ-TREE: a fast and effective stochastic algorithm for estimating maximum-likelihood phylogenies. Mol Biol Evol. 2015 Jan;32(1):268–74.

29. Letunic I, Bork P. Interactive Tree Of Life (iTOL) v4: recent updates and new developments. Nucleic Acids Res. 2019 Jul 2;47(W1):W256–9.

30. Oksanen J, Blanchet FG, Kindt R, Legendre P, Minchin P. The vegan package: Community Ecology Package. R package version 2.0--2. 2011 Jan 1;

31. Core Team R, Others. R: A language and environment for statistical computing. Vienna, Austria: R Foundation for Statistical Computing. Available. 2013;

32. Bray JR, Curtis JT. An ordination of upland forest communities of southern Wisconsin. Ecological Monographs (27). Change in Marine Communities: An Approach to Statistical Analysis and Interpretation. PRIMER-E Plymouth; 1957. p. 325–49.

33. Clarke KR, Ainsworth M. A method of linking multivariate community structure to environmental variables. Marine Ecology-Progress Series. 1993;92:205–205.

34. Fisher RA. XV.—The Correlation between Relatives on the Supposition of Mendelian Inheritance. Earth Environ Sci Trans R Soc Edinb. 1919;52(2):399–433.

35. Mielke PW, Berry KJ, Johnson ES. Multi-response permutation procedures for a priori classifications [Internet]. Vol. 5, Communications in Statistics - Theory and Methods. 1976. p. 1409–24. Available from: http://dx.doi.org/10.1080/03610927608827451

36. Darling AE, Jospin G, Lowe E, Matsen FA 4th, Bik HM, Eisen JA. PhyloSift: phylogenetic analysis of genomes and metagenomes. PeerJ. 2014 Jan 9;2:e243.

37. Parks DH, Imelfort M, Skennerton CT, Hugenholtz P, Tyson GW. CheckM: assessing the quality of microbial genomes recovered from isolates, single cells, and metagenomes. Genome Res. 2015 Jul;25(7):1043–55.

38. Kalyaanamoorthy S, Minh BQ, Wong TKF, von Haeseler A, Jermiin LS. ModelFinder: fast

model selection for accurate phylogenetic estimates. Nat Methods. 2017 Jun;14(6):587–9.

39. Wang H-C, Minh BQ, Susko E, Roger AJ. Modeling Site Heterogeneity with Posterior Mean Site Frequency Profiles Accelerates Accurate Phylogenomic Estimation. Syst Biol. 2018 Mar 1;67(2):216–35.

40. Hoang DT, Chernomor O, von Haeseler A, Minh BQ, Vinh LS. UFBoot2: Improving the Ultrafast Bootstrap Approximation. Mol Biol Evol. 2018 Feb 1;35(2):518–22.

41. Guindon S, Dufayard J-F, Lefort V, Anisimova M, Hordijk W, Gascuel O. New algorithms and methods to estimate maximum-likelihood phylogenies: assessing the performance of PhyML 3.0. Syst Biol. 2010 May;59(3):307–21.

42. Jain C, Rodriguez-R LM, Phillippy AM, Konstantinidis KT, Aluru S. High throughput ANI analysis of 90K prokaryotic genomes reveals clear species boundaries. Nat Commun. 2018 Nov 30;9(1):5114.

43. Xu L, Dong Z, Fang L, Luo Y, Wei Z, Guo H, et al. OrthoVenn2: a web server for whole-genome comparison and annotation of orthologous clusters across multiple species. Nucleic Acids Res. 2019 Jul 2;47(W1):W52–8.

44. Placzek C, Granger DE, Matmon A, Quade J, Ryb U. Geomorphic process rates in the central Atacama Desert, Chile: Insights from cosmogenic nuclides and implications for the onset of hyperaridity [Internet]. Vol. 314, American Journal of Science. 2014. p. 1462–512. Available from: http://dx.doi.org/10.2475/10.2014.03

45. Azua-Bustos A, González-Silva C, Fernández-Martínez MÁ, Arenas-Fajardo C, Fonseca R, Martín-Torres FJ, et al. Aeolian transport of viable microbial life across the Atacama Desert, Chile: Implications for Mars. Sci Rep. 2019 Aug 22;9(1):11024.

46. Mincer TJ, Church MJ, Taylor LT, Preston C, Karl DM, DeLong EF. Quantitative distribution of presumptive archaeal and bacterial nitrifiers in Monterey Bay and the North Pacific Subtropical Gyre. Environ Microbiol. 2007 May;9(5):1162–75.

47. Merbt SN, Stahl DA, Casamayor EO, Martí E, Nicol GW, Prosser JI. Differential photoinhibition of bacterial and archaeal ammonia oxidation. FEMS Microbiol Lett. 2012 Feb;327(1):41–6.

48. Church MJ, DeLong EF, Ducklow HW, Karner MB, Preston CM, Karl DM. Abundance and distribution of planktonicArchaeaandBacteriain the waters west of the Antarctic Peninsula [Internet]. Vol. 48, Limnology and Oceanography. 2003. p. 1893–902. Available from: http://dx.doi.org/10.4319/lo.2003.48.5.1893

49. Smith JM, Chavez FP, Francis CA. Ammonium Uptake by Phytoplankton Regulates Nitrification in the Sunlit Ocean [Internet]. Vol. 9, PLoS ONE. 2014. p. e108173. Available from: http://dx.doi.org/10.1371/journal.pone.0108173

50. Tolar BB, Powers LC, Miller WL, Wallsgrove NJ, Popp BN, Hollibaugh JT. Ammonia Oxidation in the Ocean Can Be Inhibited by Nanomolar Concentrations of Hydrogen

Peroxide [Internet]. Vol. 3, Frontiers in Marine Science. 2016. Available from: http://dx.doi.org/10.3389/fmars.2016.00237

51. Georgiou CD, Sun HJ, McKay CP, Grintzalis K, Papapostolou I, Zisimopoulos D, et al. Evidence for photochemical production of reactive oxygen species in desert soils. Nat Commun. 2015 May 11;6:7100.

52. Reich M, Bao H. Nitrate Deposits of the Atacama Desert: A Marker of Long-Term Hyperaridity [Internet]. Vol. 14, Elements. 2018. p. 251–6. Available from: http://dx.doi.org/10.2138/gselements.14.4.251

53. Stahl DA, de la Torre JR. Physiology and Diversity of Ammonia-Oxidizing Archaea [Internet]. Vol. 66, Annual Review of Microbiology. 2012. p. 83–101. Available from: http://dx.doi.org/10.1146/annurev-micro-092611-150128

54. Kobayashi S, Hira D, Yoshida K, Toyofuku M, Shida Y, Ogasawara W, et al. Nitric Oxide Production from Nitrite Reduction and Hydroxylamine Oxidation by Copper-containing Dissimilatory Nitrite Reductase (NirK) from the Aerobic Ammonia-oxidizing Archaeon, Nitrososphaera viennensis. Microbes Environ. 2018 Dec 28;33(4):428–34.

55. Alves RJE, Minh BQ, Urich T, von Haeseler A, Schleper C. Unifying the global phylogeny and environmental distribution of ammonia-oxidising archaea based on amoA genes. Nat Commun. 2018 Apr 17;9(1):1517.

56. Alves RJE, Kerou M, Zappe A, Bittner R, Abby SS, Schmidt HA, et al. Ammonia Oxidation by the Arctic Terrestrial Thaumarchaeote Nitrosocosmicus arcticus Is Stimulated by Increasing Temperatures. Front Microbiol. 2019 Jul 17;10:1571.

57. Jung M-Y, Kim J-G, Sinninghe Damsté JS, Rijpstra WIC, Madsen EL, Kim S-J, et al. A hydrophobic ammonia-oxidizing archaeon of the Nitrosocosmicus clade isolated from coal tar-contaminated sediment. Environ Microbiol Rep. 2016 Dec;8(6):983–92.

58. Liu L, Li S, Han J, Lin W, Luo J. A Two-Step Strategy for the Rapid Enrichment of Nitrosocosmicus-Like Ammonia-Oxidizing Thaumarchaea [Internet]. Vol. 10, Frontiers in Microbiology. 2019. Available from: http://dx.doi.org/10.3389/fmicb.2019.00875

59. Liang R, Lau MCY, Saitta ET, Garvin ZK, Onstott TC. Genome-centric resolution of novel microbial lineages in an excavated Centrosaurus dinosaur fossil bone from the Late Cretaceous of North America. Environmental Microbiome. 2020 Mar 19;15(1):8.

60. Sauder LA, Albertsen M, Engel K, Schwarz J, Nielsen PH, Wagner M, et al. Cultivation and characterization of Candidatus Nitrosocosmicus exaquare, an ammonia-oxidizing archaeon from a municipal wastewater treatment system. ISME J. 2017 May;11(5):1142–57.

61. Meier-Kolthoff JP, Auch AF, Klenk H-P, Göker M. Genome sequence-based species delimitation with confidence intervals and improved distance functions. BMC Bioinformatics. 2013 Feb 21;14:60.

62. Goris J, Konstantinidis KT, Klappenbach JA, Coenye T, Vandamme P, Tiedje JM. DNA--

669 DNA hybridization values and their relationship to whole-genome sequence similarities. Int
670 J Syst Evol Microbiol. 2007;57(1):81–91.

671 63. Konstantinidis KT, Rosselló-Móra R, Amann R. Uncultivated microbes in need of their own
672 taxonomy. ISME J. 2017 Nov;11(11):2399–406.

673 64. Lebre PH, De Maayer P, Cowan DA. Xerotolerant bacteria: surviving through a dry spell.
674 Nat Rev Microbiol. 2017 May;15(5):285–96.

675 65. Moreno ML, Piubeli F, Bonfá MRL, García MT, Durrant LR, Mellado E. Analysis and
676 characterization of cultivable extremophilic hydrolytic bacterial community in heavy-metal-
677 contaminated soils from the Atacama Desert and their biotechnological potentials. J Appl
678 Microbiol. 2012 Sep;113(3):550–9.

679 66. Calamita G. The Escherichia coli aquaporin-Z water channel: MicroReview. Mol Microbiol.
680 2000;37(2):254–62.

681 67. Wang B, Qin W, Ren Y, Zhou X, Jung M-Y, Han P, et al. Expansion of Thaumarchaeota
682 habitat range is correlated with horizontal transfer of ATPase operons. ISME J. 2019
683 Dec;13(12):3067–79.

684 68. Zhong H, Lehtovirta-Morley L, Liu J, Zheng Y, Lin H, Song D, et al. Novel insights into the
685 Thaumarchaeota in the deepest oceans: their metabolism and potential adaptation
686 mechanisms. Microbiome. 2020 Jun 1;8(1):78.

687

688 **Supplementary Information for:**
689
690 **Leave no stone unturned: The hidden potential of carbon and nitrogen cycling by novel, highly**
691 **adapted *Thaumarchaeota* in the Atacama Desert hyperarid core**
692
693 Yunha Hwang[1], Dirk Schulze-Makuch[1*], Felix L. Arens[1], Johan S. Saenz[3], Panagiotis S. Adam[2],
694 Till L.V. Bornemann[2], Alessandro Airo[1], Michael Schloter[3], Alexander J. Probst[2*]
695
696 *corresponding authors

697 **Affiliations:**
698 [1] Center of Astronomy & Astrophysics, Technical University Berlin, 10623, Berlin, Germany
699 [2] Environmental Microbiology and Biotechnology, Department of Chemistry, University of
700 Duisburg-Essen, 45141, Essen, Germany
701 [3] Research Unit for Comparative Microbiome Analysis, Helmholtz Zentrum München, 85758,
702 Oberschleißheim, Germany
703
704 To whom the correspondence should be addressed:
705 alexander.probst@uni-due.de
706 schulze-makuch@tu-berlin.de
707
708
709 **List of Content:**
710 - Supplementary Materials and Methods (M1-M7)
711 - Supplementary Results and Discussion
712 - Figures S1-S12 and Tables S1 and S2
713 - Legends for Supplementary Tables S3-14
714 - Descriptions for additional Supplementary File
715

Supplementary Materials and Methods

M1. Field measurements

The HOBO U23 pro Temperature/Relative Humidity data logger (Onset, Cat# U23-001, MA, USA) was used to monitor the temperature and relative humidity of each site at the time of sampling. For each sampling site (Y, M, L), an extra boulder was chosen for conducting HOBO logger measurements. One logger was placed under a boulder similarly sized to those chosen for sampling, and another logger was placed ~20 cm away from the boulder on the open soil. For the Y site, a continuous measurement over 130 days (15 March - 25 July 2019) was conducted for characterizing diurnal fluctuations for both below boulder, beside boulder and 1 m above ground. Logged data was then used to calculate dew point temperatures as described in Lawrence *et al. (1)*.

M2. pH and electrical conductivity

To evaluate the pH and the electric conductivity (EC) of the soil, samples were prepared in a ratio 1:5 v/v (5 ml sample to 25 ml distilled water), shaken for one hour to prevent the particle from settling and sedimented for another hour, before measuring pH (691 pH Meter, Metrohm, Switzerland). The standard deviation was determined by repeated measurements of in-house standards, SD = 0.24 (n = 16). EC was measured with a handheld electric conductivity meter (GMH 3400, Greisinger, Germany). Reproducibility variation was 5% (n = 3). Both measurements were conducted at the Center of Astronomy and Astrophysics the Technische Universität Berlin.

M3. Anion and cation analysis

Samples and processing controls for water-soluble ion analysis were prepared based on the standard DIN EN 12457 - 4 (2003) protocol. Briefly, samples were sieved to obtain <2 mm particles which were used to prepare an eluate of a 1:10 w/w (4.5 g sample to 45 g distilled water). After 24 h of continuous shaking, the eluate was filtered through 0.2 µm mesh and stored at -20°C until measurement. Anionic species (Cl^-, NO_3^-, PO_4^{3-}, SO_4^{2-}) were measured by ion chromatography (DIONEX DX-120 Ion chromatograph, Thermo Fisher Scientific, USA, with a guard column AG 22, 4x50 mm and an analytical column AS 22, 4x250 mm). Reproducibility variation was <1% (n = 5). Cations (Ca^{2+}, Fe^{2+}, K^+, Mg^{2+}, Mn^{2+}, Na^+) were determined by inductively-coupled plasma optical emission spectrometry (iCAP 6000 ICP Spectrometer, Thermo Fisher Scientific, USA). Reproducibility variation was <5% (n = 5). Both analyses were conducted at the Department of Soil Science of the Technische Universität Berlin. Bray-Curtis distance ("vegan" package (2)) metric was used to calculate the distance matrix of samples based on the ion concentrations, which was then used for non-metric multidimensional scaling analysis in R (3).

M4. Total organic carbon analysis

The total organic carbon (TOC) was measured with an elemental analyzer (Vario Max C, Elementar, Germany) using catalytic tube combustion at the Department of Life Science of the Humboldt Universität Berlin. Samples were first ground to powder. Due to low TOC concentrations, 1 g was used for combustion. At 600°C the organic carbon was removed under the carrier gas nitrogen and oxidized by oxygen in the presence of copper oxide. Remaining elemental carbon was combusted with the addition of oxygen. The resulting CO_2 was then determined successively by infrared detection. The measurement was conducted in duplicates with a detection

762 limit of 0.0124 wt%.

763 **M5. Bulk mineralogy**
764 For the bulk mineralogy, soil samples were homogenized and ground to powder. X-ray powder
765 diffraction (XRD) analysis of the soil salts was performed by using a powder diffractometer (D2
766 Phaser, Bruker, USA) at the Department of Applied Geochemistry of the Technische Universität
767 Berlin. The X-ray source was Cu Kα radiation (K-alpha1 = 1.540598 Å, K-alpha2 =1.54439 Å)
768 with a performance of 30 kV and 10 mA. A step interval of 0.013° 2Θ with a step-counting time
769 of 0.5 s was used in a scanning range from 3° to 80° 2Θ. Semi-quantitative mineral content was
770 calculated based on relative intensity values using the software package DIFRAC.EVA V2
771 (Bruker, USA). Absolute reproducibility variation was < 1% (n = 4).
772
773 **M6. DNA extraction, Illumina library preparation and sequencing**
774 Metagenomic DNA was extracted from 10 g of soil as described previously (4). Briefly, the soil
775 was mixed for 30 minutes in 40 mL cell extraction buffer (1% PEG 8000 ; 1M NaCl, pH 9,2) (5).
776 The supernatant was ultra-centrifuged 2 h at 44,000 x g at 4 °C and DNA was extracted from the
777 pellet using a bead-beating and phenol/chloroform/isoamylalcohol based protocol (6). DNA was
778 resuspended in 30 µL of DEPC treated water. Two extractions were performed per sample and the
779 resulting DNA was combined. DNA concentration was measured using the Qubit 1x dsDNA HS
780 Assay Kit (Thermo Fisher Scientific) and Qubit 4 Fluorometer (Thermo Fisher Scientific). 10 mL
781 of the cell extraction buffer was used as a negative control for DNA extraction.
782
783 Approximately 5-15 ng of DNA were shared with a E220 Focused-ultrasonicator (Covaris® Inc.,
784 MA, USA), targeting 300-400 fragment size, and used to prepare the metagenomic libraries. The
785 libraries were constructed using the NEBNEXT® ultra II DNA library prep kit for Illumina and
786 the NEBNext® primer set 1 (Dual index, New England BioLabs, UK) with three modifications.
787 1) the primer adapters were diluted 1:50 v/v, 2) the primers were diluted 1:2 v/v and 3) a second
788 cleaning step was performed after PCR amplification. Purification and size selection were
789 conducted using magnetic beads Agencourt® AMPure® XP (Beckman-Coulter, MA, USA).
790 Inserts between 400 and 500 bp were kept and their quality evaluated using a Fragment Analyzer™
791 (Advanced Analytical, IA, USA). Library concentration was measured with the Qubit 1x dsDNA
792 HS Assay Kit and Qubit 4 Fluorometer. The metagenomic libraries were sequenced on an Illumina
793 HiSeq 2500 (Illumina, CA, USA) using the HiSeq Rapid SBS Kit v2 (500 cycles, Illumina, CA,
794 USA) and loading 12 pM including 1% v/v PhiX.
795
796 **M7. Metagenome assembly, binning and annotation**
797 HiSeq reads were quality filtered using BBduk (https://sourceforge.net/projects/bbmap/) and
798 sickle (https://github.com/najoshi/sickle). metaSPADES 3.13 (7) was used to assemble the reads
799 and the resulting scaffolds were filtered for length >= 1000 bp for gene prediction using Prodigal
800 (8) in meta mode and annotation using Diamond version 0.9.9 (9) against the UniRef100 database
801 (10) with e-value cut-off of 1E-5. Scaffold coverages were calculated by mapping reads using
802 Bowtie2 in sensitive mode (11). Genomes were binned using abawaca
803 (github.com/CK7/abawaca), ESOM (12) and MaxBin2 (13), and the resulting bins were
804 aggregated using DAS Tool (14). Each genomic bin was manually curated using coverage, gene-
805 based taxonomy and GC content information for each scaffold. ra2 (15) was used to fix assembly
806 errors in all binned scaffolds. CheckM (16) was used to estimate the quality of the bins and only
807 high quality bins with completeness >75% and contamination <15% were considered for further

808 analysis. For all high quality genomes, GTDB-Tk classify_wf (17) was used for a broad taxonomic
809 classification and *in situ* genome replication measures (iRep) (18) were calculated using --mm 3
810 flag after mapping the reads to scaffolds with Bowtie2 (19). Further functional and metabolic
811 capacities of high quality genomes and metagenomes were determined using METABOLIC (20).
812 METABOLIC output was further expanded upon using hidden-markov-model (HMM) search
813 results for the archaeal amoA protein (HMMER v3.2 (http://hmmer.org/), -Z 47079205 -E 1000)
814 and other genes previously annotated using the UniREF100 database (10). Relative abundances of
815 key metabolic genes were calculated by identifying scaffolds carrying the gene in question,
816 summing up their coverages and finally normalizing the summed coverage with the sequencing
817 depth of each respective sample.
818

Supplementary Results and Discussion

Extended pangenome analysis

Notably, none of the eight Thaumarchaeota genomes contained CRISPR arrays with more than one spacer and only ABT-LB2 contained a putative *cas* gene. Similarly no Cas gene was found in *N. franklandus, N. oleophilus* and *N. exaquare*, and one Cas gene was found in N. arcticus. Only *N. exaquare* contained an evidence level 4 CRISPR array with 5 spacers (**Table S11**). The lack of CRISPR-Cas systems in these environments could be due to the lower presence of *Thaumarchaeota* targeting viruses in these environments and/or be coupled with slow growth rates rendering the CRISPR-Cas system immune response ineffective (21).

Electron transfer flavoprotein fixABCX genes were found only amongst the ABT genomes and not in any of *Ca. Nitrosocosmici* (**Table S11**). These genes are reported to be involved in the electron bifurcation in diazotrophs (22), but are also found in many non-diazotrophic *Archaea* (23), where their function is yet to be determined.

No S-layer protein slp1 was found in any of the ABT nor other *Ca. Nitrosocosmici*. The presence of Hexuronic acid methyltransferase AglP, which is involved in the pathway of S-layer biogenesis, suggests that there may exist an alternative pathway for S-layer production. This could provide additional protection against harsh desert environments for the ABT genomes (24).

Supplementary Figures and Tables

Table S1: Sampling information, temperature and relative humidity below and beside boulders were measured using OBO U23 pro temperature/relative humidity data logger at the time of sampling.

Site	Location Name	Longitude	Latitude	Altitude (m above sea level)	Temp - Below (°C)	Temp - Beside (°C)	Relative Humidity - Below (%)	Relative Humidity - Beside (%)	Collection Time (+/- 15 min)	Collection Date
Y	Yungay	-69.99927	-24.08663	1067	22.29	33.55	31.81	21.24	11:00:00 AM	10/3/2019
M	Maria Elena	-69.72428	-22.26319	1318	18.6	14.3	32.6	68.4	8:30:00 AM	13/3/2019
L	Lomas Bayas	-69.60378	-23.39321	1521	36.25	37.53	11.91	13.71	12:30:00 PM	13/3/2019

Table S2. Metagenome library information. DNA extracts from MB6, MC3, YB2 and YB5 contained measurable DNA (see **Figure S1**) however, failed in library preparation.

Library	Reads (bp)	Assembly size (bp)	# scaffolds	# scaffolds >=1000bp	N50 (scaffolds >=1000bp by length)	Sequencing depth	NCBI Accession ID
LB2	22,130,842	303,328,226	529,525	53,921	748	9,768,467,534	XXXXXX
LB3	31,273,647	388,980,799	619,007	73,975	934	13,479,472,613	XXXXXX
LB5	42,100,542	27,9268,968	502,503	46,030	644	18,239,942,017	XXXXXX
LC2	41,952,484	390,674,555	678,127	74,711	1,058	16,737,394,618	XXXXXX
LC3	20,973,878	385,836,147	692,036	72,209	820	9,268,440,081	XXXXXX
LC5	36,938,861	498,167,674	1,001,606	80,101	660	15,452,539,821	XXXXXX
MB1	50,912,651	397,090,821	724,094	64,247	606	21,951,582,505	XXXXXX
MB3	13,796,379	325,366,862	602,775	55,520	621	5,836,722,551	XXXXXX
MB4	36,370,037	490,933,896	960,960	74,205	572	16,170,303,555	XXXXXX
YB1	15,371,532	295,824,573	499,610	54,472	721	6,539,418,086	XXXXXX
YB3	27,738,528	335,124,123	571,894	58,118	693	12,052,827,536	XXXXXX

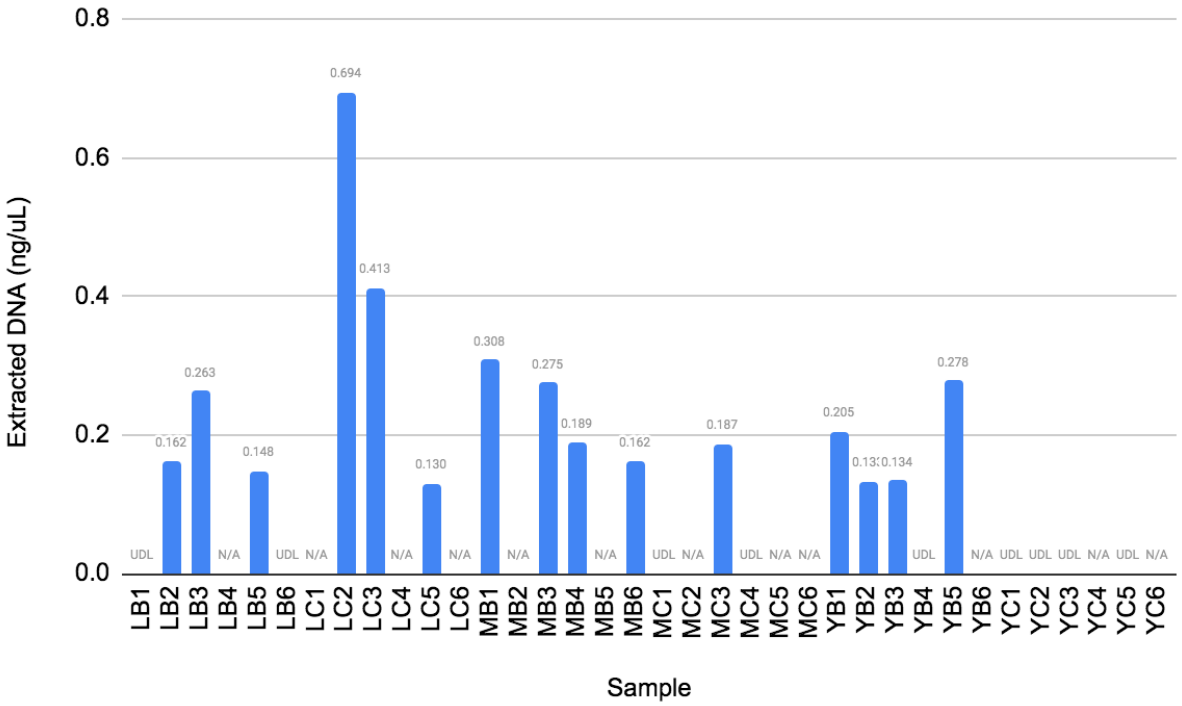

Figure S1. DNA extraction results. UDL (under detection limit) indicates extraction was attempted but resulted in DNA amount below detection limit (0.01 ng/uL) and N/A indicates no extraction was attempted.

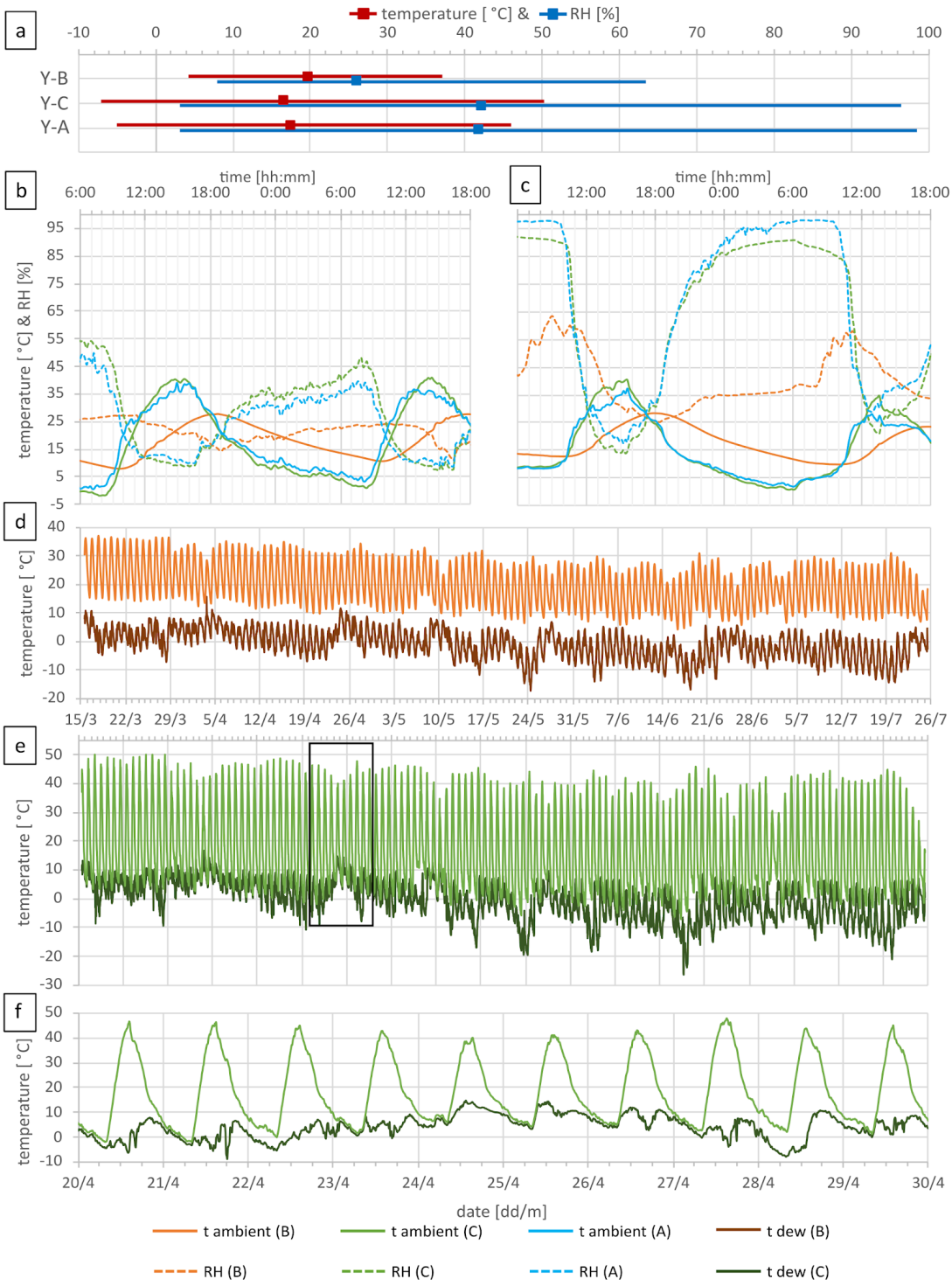

Figure S2. Extended field measurements of temperature and relative humidity (RH) for Y-below boulder (B), control (C) and in 1 m above ground (A). a) Mean temperature and RH (square) and range (bar). b) Temperature and RH during a dry diurnal cycle; c) Temperature and RH during a moist diurnal cycle. d) Ambient temperature and calculated dew point temperature below boulder (B) during the full 130 days of recording. e) Ambient temperature and calculated

863 dew point temperature beside boulder (control) during the full 130 days of recording, black
864 rectangle is zoomed in panel f).
865

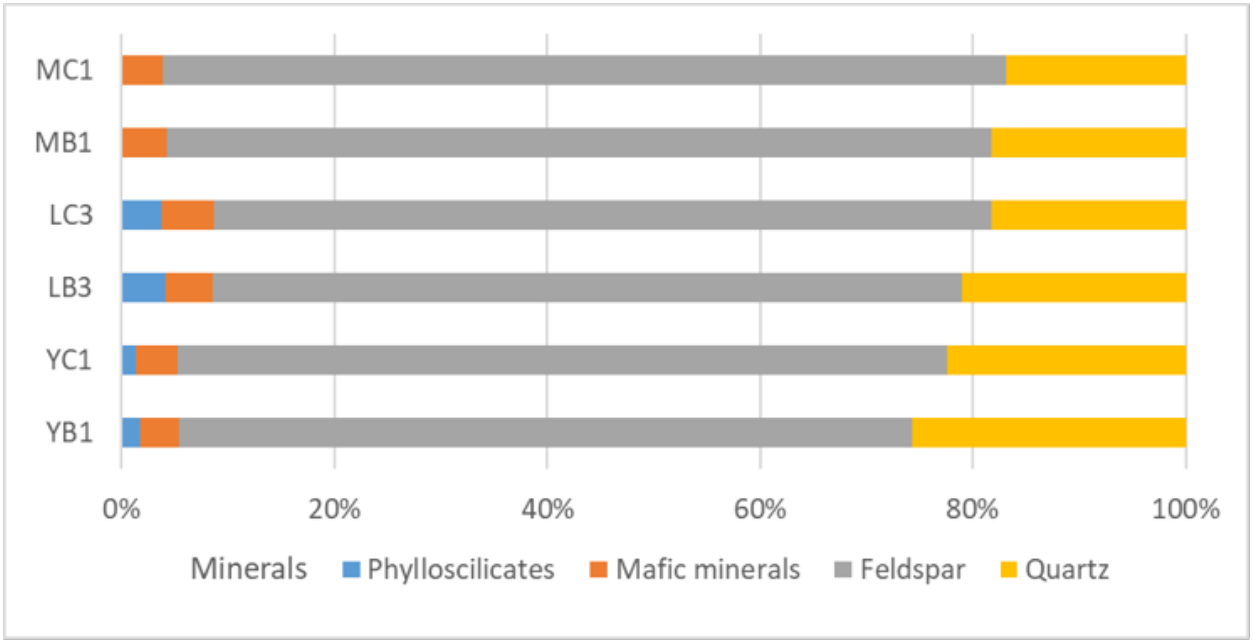

866
867 **Figure S3. Mineral composition determined using XRD.**

a)

b)

Figure S4. Atacama Boulder Fields. a) Yungay Valley boulder field. b) An example of the boulders chosen for sampling.

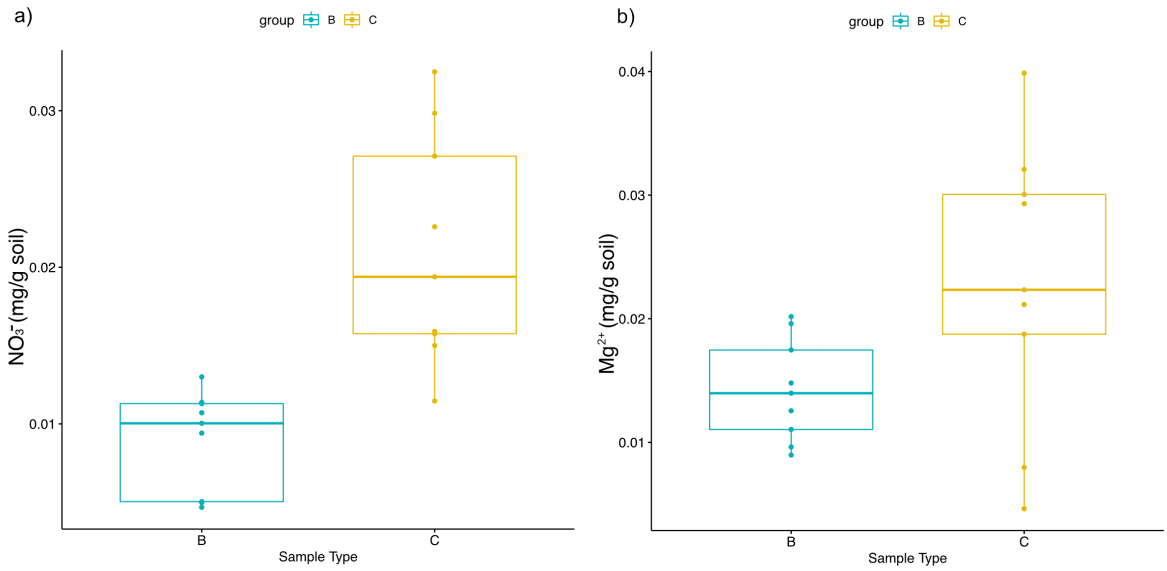

Figure S5. Comparison of a) nitrate and b) magnesium ion concentrations between B and C sample types. Plots were visualized using "ggpubr" package in R.

874

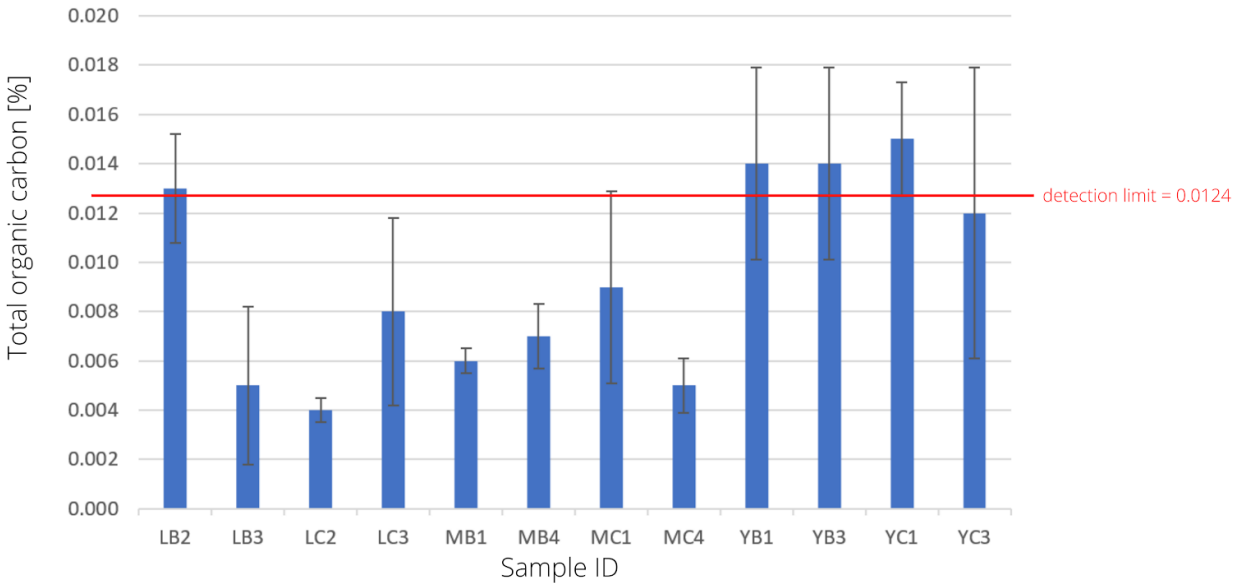

875

876 **Figure S6. Total Organic Carbon (TOC) content [wt%] per sample.** All values were below
877 the limit of quantitation value 0.02962 wt% and very close to or below the limit of detection 0.0124
878 wt%.

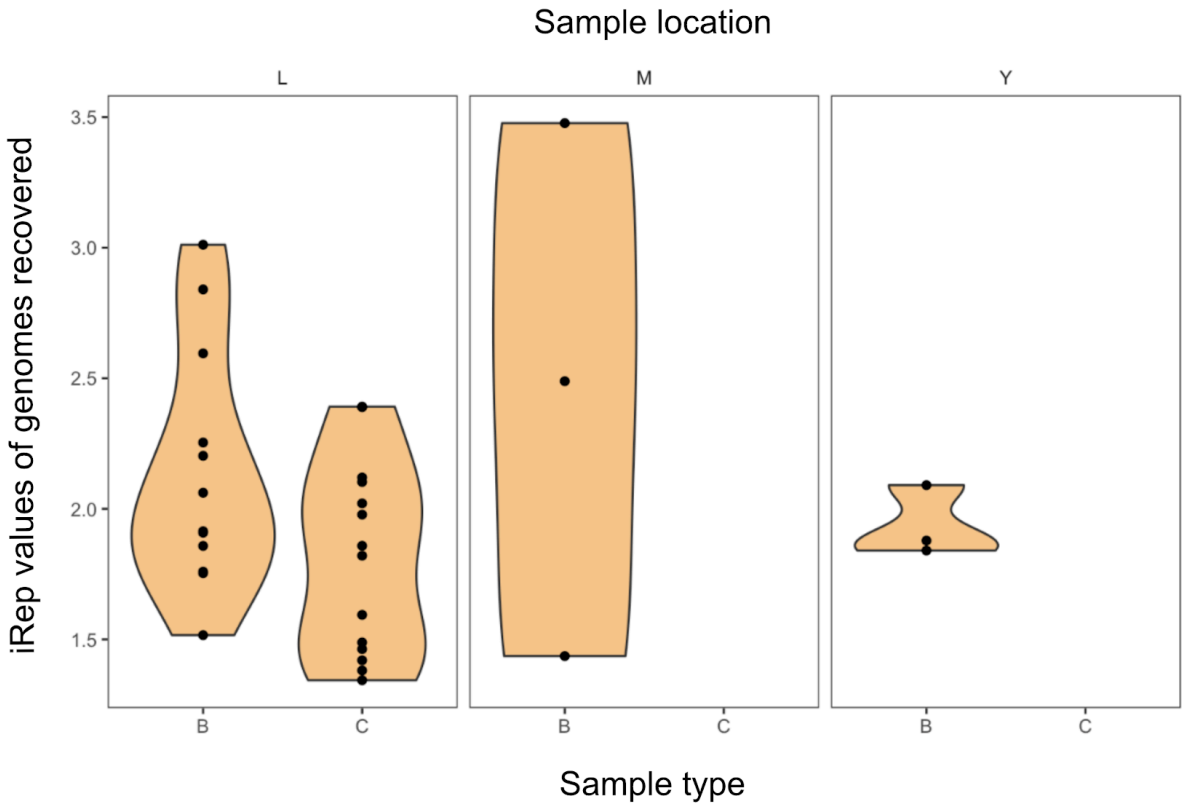

Figure S7. calculated iRep values of genomes of sample type (B and C) and sample sites (L, M and Y). Plot was visualized using ggplot2 (25)

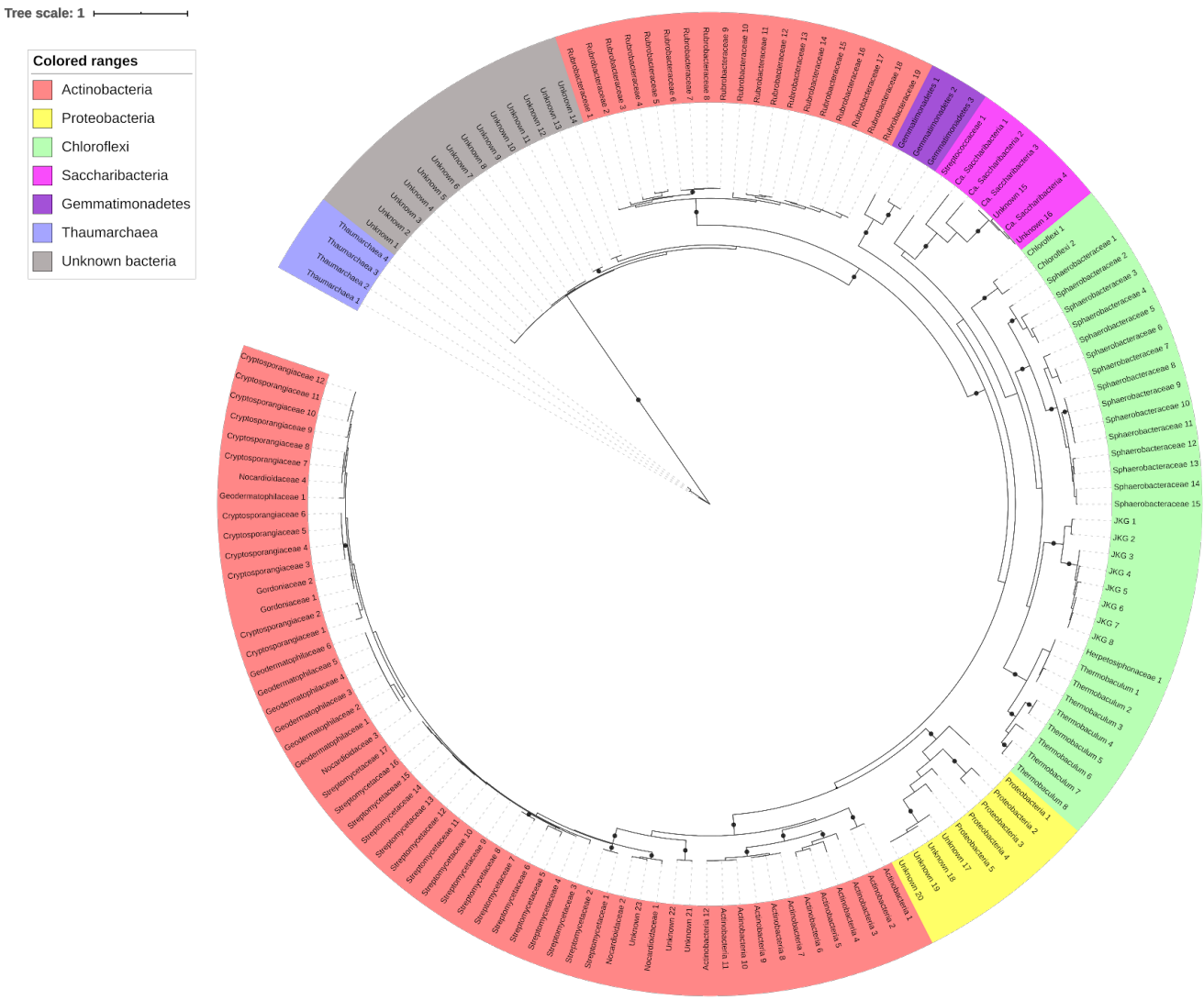

Figure S8. Full phylogenetic tree of all recovered rpS3 gene clusters. Color ranges refer to phyla level classification, leaf labels refer to taxonomic resolution down to family level based on BLAST (26) results against UniRef100 (10). Strongly supported branches as described in the Methods section are indicated with black dots.

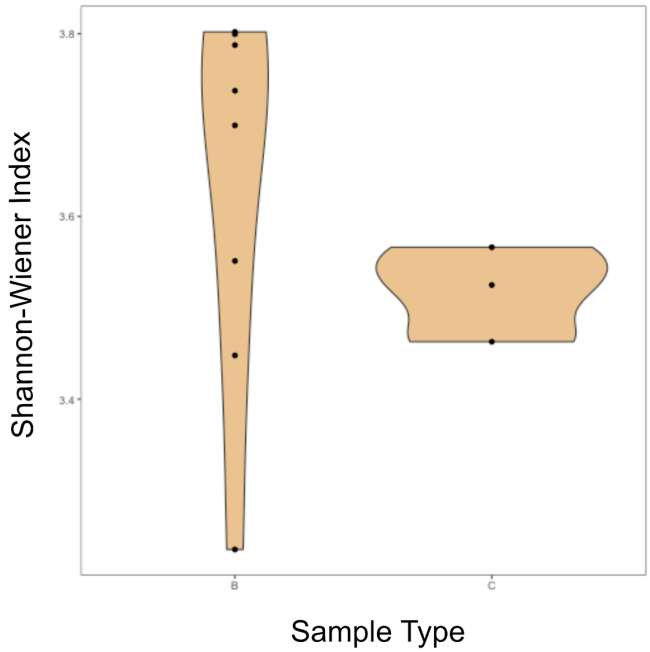

Figure S9. Shannon-Wiener index of each metagenome. Indices were calculated based on normalized ribosomal protein S3 (rpS3) abundances. Plot was visualized using ggplot2 (25).

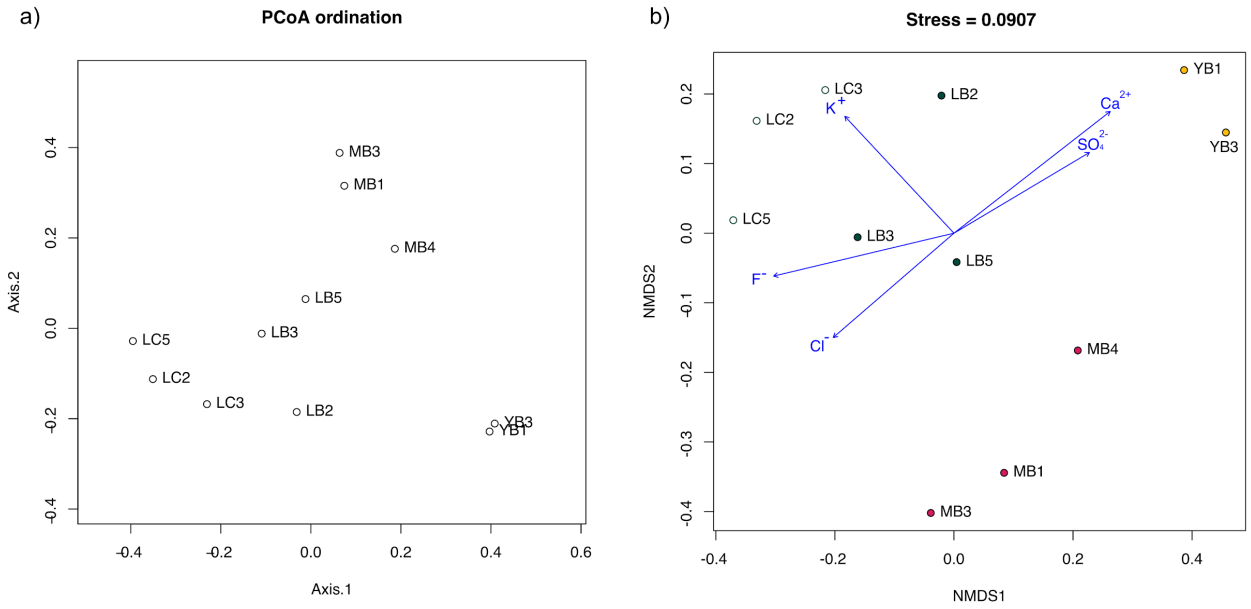

Figure S10. a) PCoA and b) NMDS ordination plots of metagenomes based on rpS3 abundances. Bray-Curtis distance matrix of normalized abundances of rpS3 taxa across all metagenomes were calculated and used as input for both figures. For NMDS, ion concentration meta data was added and the vectors were fitted with the ordination. Blue arrows represent fitted ion species with a p-value less than 0.1. Both figures were generated using R.

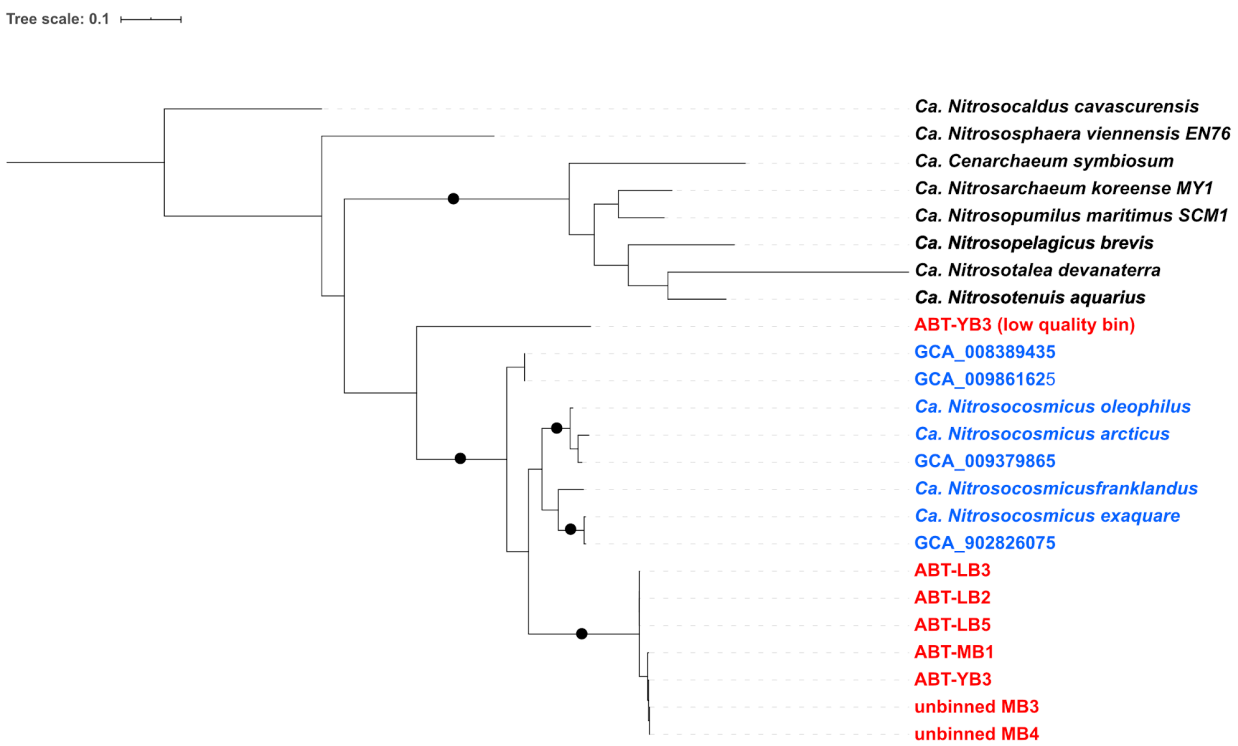

Figure S11. Tree of all *amoA* sequences from this study (red), *amoA*s from *Ca. Nitrosocosmicus* (Blue) and other representative Thaumarchaea sequences (Black). Strongly supported branches as described in the M&M section are indicated with black dots.

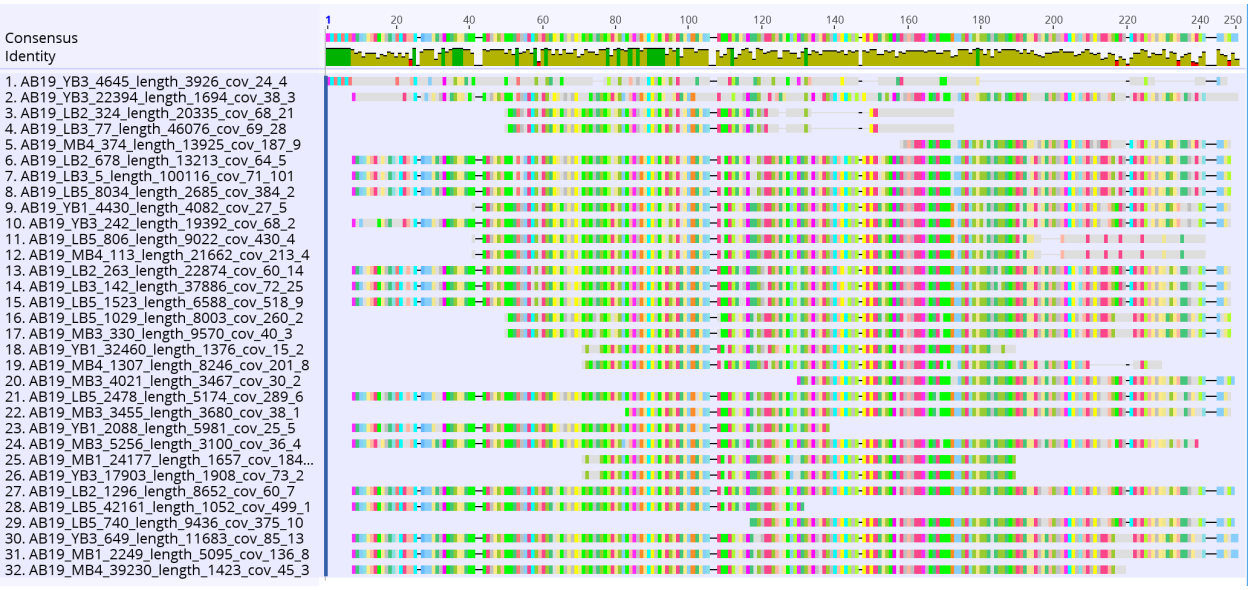

Figure S12. Alignments of 32 aquaporins recovered across all samples. Visualization using the Geneious software. Sequences 1-4 show a high level of sequence divergence, while the rest show truncation at both ends despite most being located mid scaffold.

912

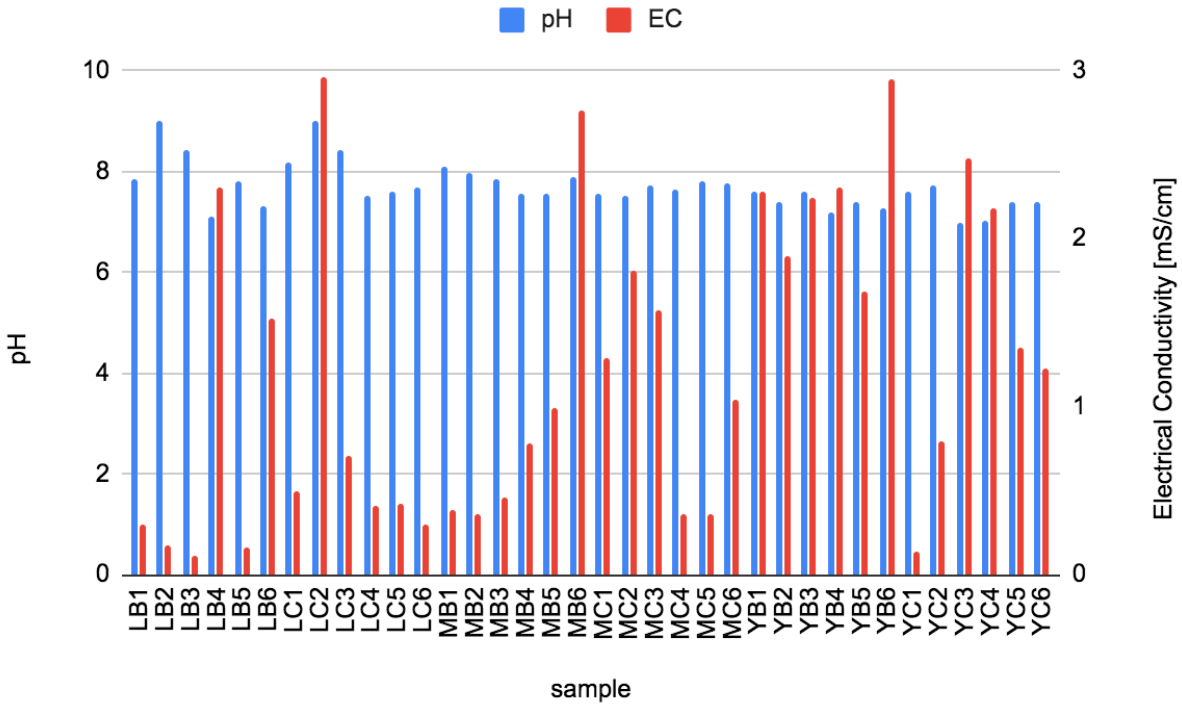

913
914 **Figure S13. pH and electrical conductivity (EC) of each sample.**

Tables S3 - S14 are available as a separate Excel file:

Table S3. Statistics and meta-data of the reference genomes used for comparative genomics.

Table S4. Genome statistics of high quality genomes. High quality genomes were determined using CheckM completeness > 75 % and contamination < 15 %. CheckM(16) output (Completeness, contamination, GC std, # ambiguous bases, Genome size, Longest Contig, N50 (scaffolds), Mean scaffold length, # contigs, # scaffolds, # predicted genes, Longestscaffold, GC, N50 (contigs), Coding density, Mean contig length) are accompanied by iRep value (18)) for genomes whose iRep values could be calculated, rpS3 taxa based on BLAST(26) results against UniRef100 database (10), gtdb-tk classification (17) using "classify_wf".

Table S5. Normalized abundances of all rpS3 taxa across all samples. Column 1 corresponds to the scaffold containing the centroid of each rpS3 cluster, which was then used to calculate the normalized abundance of each rpS3 cluster (taxa) across all samples.

Table S6. ANOVA p-values of all rpS3 taxa. For all 147 rpS3 taxa ANOVA tests were performed between Boulder and Control sample groups (B x C), YB and MB samples (YB x MB), YB and LB samples (YB x LB), and LB and MB samples (LB x MB)

Table S7. METABOLIC output of metagenomes. Presence, count and gene ID of all the predicted metabolic genes found across the metagenome.

Table S8. METABOLIC output of all high quality genomes. Presence, count and gene ID of all the predicted metabolic genes found across the metagenome.

Table S9. Ammonification genes.

Table S10. Orthologous protein clusters with GO (27,28) **and Swiss-Prot**(29) **annotation.** Clusters were determined using Orthovenn2(30). In orange are clusters with putative functions associated with stress response and in yellow are clusters with putative functions associated with nitrogen metabolism.

Table S11. List of amoABCX genes, 4HB/3HP pathway genes, TCA cycle, gluconeogenesis, pentose phosphate pathway and other notable genes for each ABT genomes.

Table S12. Singletons of LB3, MB4, YB3 genomes. Singletons were identified using Orthovenn2(30) and annotated by BLASTing (26,30) against UniRef100 database (10)

Table S13. List of NCBI genomes used for phylogenomic tree construction. NCBI genomes classified as Thaumarchaeota on 30th May 2020, filtered using CheckM completeness >50 % and contamination < 5%.

Table S14. Ion chromatography raw data in mg/g soil.

961
962
963
964
965
966
967 **Additional File:**
968
969 **Additional File 1**: Newick treefile of *Ca. Nitrosodesertus* and NCBI genomes annotated as
970 *Thaumarchaeaota*

Supplementary references

1. Lawrence MG. The Relationship between Relative Humidity and the Dewpoint Temperature in Moist Air: A Simple Conversion and Applications. Bull Am Meteorol Soc. 2005 Feb 1;86(2):225–34.

2. Oksanen J, Blanchet FG, Kindt R, Legendre P, Minchin P. The vegan package: Community Ecology Package. R package version 2.0--2. 2011 Jan 1;

3. Core Team R, Others. R: A language and environment for statistical computing. Vienna, Austria: R Foundation for Statistical Computing. Available. 2013;

4. Schulze-Makuch D, Wagner D, Kounaves SP, Mangelsdorf K, Devine KG, de Vera J-P, et al. Transitory microbial habitat in the hyperarid Atacama Desert. Proc Natl Acad Sci U S A. 2018 Mar 13;115(11):2670–5.

5. Narayan A, Jain K, Shah AR, Madamwar D. An efficient and cost-effective method for DNA extraction from athalassohaline soil using a newly formulated cell extraction buffer. 3 Biotech. 2016 Jun;6(1):62.

6. Improved protocol for the simultaneous extraction and column-based separation of DNA and RNA from different soils. J Microbiol Methods. 2011 Mar 1;84(3):406–12.

7. Nurk S, Meleshko D, Korobeynikov A, Pevzner PA. metaSPAdes: a new versatile metagenomic assembler. Genome Res. 2017 May;27(5):824–34.

8. Hyatt D, Chen G-L, Locascio PF, Land ML, Larimer FW, Hauser LJ. Prodigal: prokaryotic gene recognition and translation initiation site identification. BMC Bioinformatics. 2010 Mar 8;11:119.

9. Buchfink B, Xie C, Huson DH. Fast and sensitive protein alignment using DIAMOND [Internet]. Vol. 12, Nature Methods. 2015. p. 59–60. Available from: http://dx.doi.org/10.1038/nmeth.3176

10. Suzek BE, Huang H, McGarvey P, Mazumder R, Wu CH. UniRef: comprehensive and non-redundant UniProt reference clusters. Bioinformatics. 2007 May 15;23(10):1282–8.

11. Langdon WB. Performance of genetic programming optimised Bowtie2 on genome comparison and analytic testing (GCAT) benchmarks. BioData Min. 2015 Jan 8;8(1):1.

12. Dick GJ, Andersson AF, Baker BJ, Simmons SL, Thomas BC, Yelton AP, et al. Community-wide analysis of microbial genome sequence signatures. Genome Biol. 2009 Aug 21;10(8):R85.

13. Wu Y-W, Simmons BA, Singer SW. MaxBin 2.0: an automated binning algorithm to recover genomes from multiple metagenomic datasets. Bioinformatics. 2016 Feb 15;32(4):605–7.

14. Sieber CMK, Probst AJ, Sharrar A, Thomas BC, Hess M, Tringe SG, et al. Recovery of genomes from metagenomes via a dereplication, aggregation and scoring strategy [Internet]. Vol. 3, Nature Microbiology. 2018. p. 836–43. Available from: http://dx.doi.org/10.1038/s41564-018-0171-1

15. Brown CT, Hug LA, Thomas BC, Sharon I, Castelle CJ, Singh A, et al. Unusual biology across a group comprising more than 15% of domain Bacteria [Internet]. Vol. 523, Nature. 2015. p. 208–11. Available from: http://dx.doi.org/10.1038/nature14486

16. Parks DH, Imelfort M, Skennerton CT, Hugenholtz P, Tyson GW. CheckM: assessing the quality of microbial genomes recovered from isolates, single cells, and metagenomes. Genome Res. 2015 Jul;25(7):1043–55.

17. Chaumeil P-A, Mussig AJ, Hugenholtz P, Parks DH. GTDB-Tk: a toolkit to classify genomes with the Genome Taxonomy Database. Bioinformatics [Internet]. 2019 Nov 15; Available from: http://dx.doi.org/10.1093/bioinformatics/btz848

18. Brown CT, Olm MR, Thomas BC, Banfield JF. Measurement of bacterial replication rates in microbial communities [Internet]. Vol. 34, Nature Biotechnology. 2016. p. 1256–63. Available from: http://dx.doi.org/10.1038/nbt.3704

19. Langmead B, Trapnell C, Pop M, Salzberg SL. Ultrafast and memory-efficient alignment of short DNA sequences to the human genome. Genome Biol. 2009 Mar 4;10(3):R25.

20. Zhou Z, Tran P, Liu Y, Kieft K, Anantharaman K. METABOLIC: A scalable high-throughput metabolic and biogeochemical functional trait profiler based on microbial genomes [Internet]. Available from: http://dx.doi.org/10.1101/761643

21. Burstein D, Sun CL, Brown CT, Sharon I, Anantharaman K, Probst AJ, et al. Major bacterial lineages are essentially devoid of CRISPR-Cas viral defence systems. Nat Commun. 2016 Feb 3;7:10613.

22. Ledbetter RN, Garcia Costas AM, Lubner CE, Mulder DW, Tokmina-Lukaszewska M, Artz JH, et al. The Electron Bifurcating FixABCX Protein Complex from Azotobacter vinelandii: Generation of Low-Potential Reducing Equivalents for Nitrogenase Catalysis. Biochemistry. 2017 Aug 15;56(32):4177–90.

23. Reji L, Francis CA. Metagenome-assembled genomes reveal unique metabolic adaptations of a basal marine Thaumarchaeota lineage. ISME J [Internet]. 2020 May 13; Available from: http://dx.doi.org/10.1038/s41396-020-0675-6

24. Nicol GW, Hink L, Gubry-Rangin C, Prosser JI, Lehtovirta-Morley LE. Genome Sequence of " Nitrosocosmicus franklandus" C13, a Terrestrial Ammonia-Oxidizing Archaeon. Microbiol Resour Announc [Internet]. 2019 Oct 3;8(40). Available from: http://dx.doi.org/10.1128/MRA.00435-19

25. Wickham H, Chang W. ggplot2: an implementation of the grammar of graphics.(0.9. 3 edn). See http://ggplot2 org. 2012;

1043 26. Altschul SF, Gish W, Miller W, Myers EW, Lipman DJ. Basic local alignment search tool. J
1044 Mol Biol. 1990 Oct 5;215(3):403–10.

1045 27. Ashburner M, Ball CA, Blake JA, Botstein D, Butler H, Michael Cherry J, et al. Gene
1046 Ontology: tool for the unification of biology [Internet]. Vol. 25, Nature Genetics. 2000. p.
1047 25–9. Available from: http://dx.doi.org/10.1038/75556

1048 28. The Gene Ontology Consortium. The Gene Ontology Resource: 20 years and still GOing
1049 strong. Nucleic Acids Res. 2019 Jan 8;47(D1):D330–8.

1050 29. Bairoch A, Apweiler R. The SWISS-PROT protein sequence database and its supplement
1051 TrEMBL in 2000. Nucleic Acids Res. 2000 Jan 1;28(1):45–8.

1052 30. Xu L, Dong Z, Fang L, Luo Y, Wei Z, Guo H, et al. OrthoVenn2: a web server for whole-
1053 genome comparison and annotation of orthologous clusters across multiple species. Nucleic
1054 Acids Res. 2019 Jul 2;47(W1):W52–8.

1055